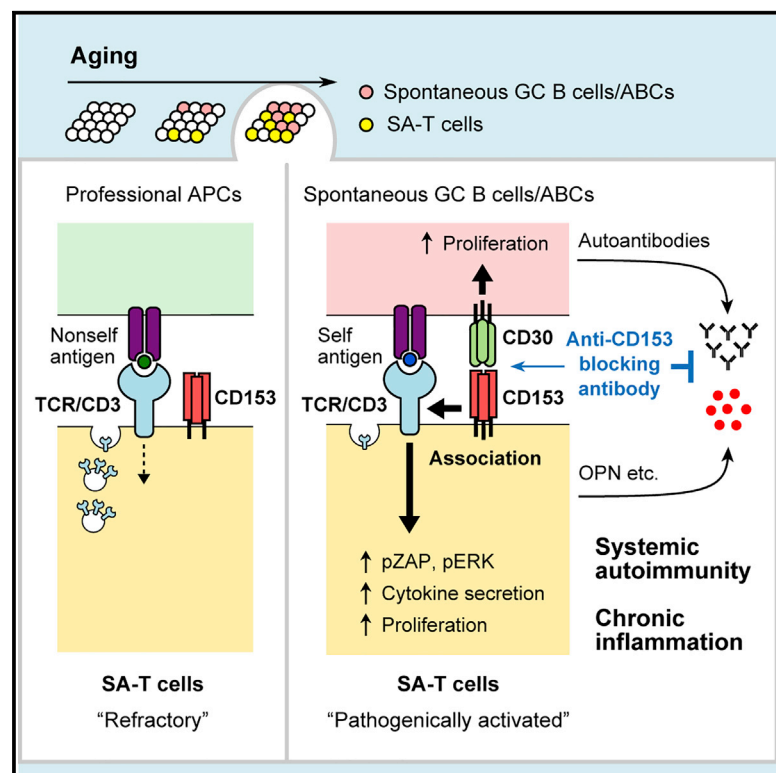# *cis* interaction of CD153 with TCR/CD3 is crucial for the pathogenic activation of senescence-associated T cells

Graphical abstract

Highlights

- *CD153*$^{-/-}$ and *CD30*$^{-/-}$ mice show reduced numbers of age-related T and B cell subsets

- CD30 signaling supports the expansion of CD30$^+$ GC B cells

- Association of CD153 with TCR/CD3 on SA-T cells enhances TCR signaling and activation

- Blockade of CD153/CD30 interaction suppresses the immunosenescent phenotype and lupus

Authors

Yuji Fukushima, Keiko Sakamoto, Michiyuki Matsuda, ..., Misaki Chihara, Nagahiro Minato, Masakazu Hattori

Correspondence

fukushima.yuji.4x@kyoto-u.ac.jp (Y.F.),
hattori.masakazu.8a@kyoto-u.ac.jp
(M.H.)

In brief

Aging may affect immunological function with increased propensity for autoimmunity. Fukushima et al. show that interaction between CD153 and CD30 causes reciprocal expansion of age-related T and B cell subsets. Association of CD153 with TCR/CD3 induces the activation of even refractory senescence-associated T cells. Antibody-mediated blockade of CD153/CD30 interaction ameliorates lupus.

Article

cis interaction of CD153 with TCR/CD3 is crucial for the pathogenic activation of senescence-associated T cells

Yuji Fukushima,[1,8,*] Keiko Sakamoto,[2] Michiyuki Matsuda,[3] Yasunobu Yoshikai,[4] Hideo Yagita,[5] Daisuke Kitamura,[6] Misaki Chihara,[1] Nagahiro Minato,[7] and Masakazu Hattori[1,*]

[1]Department of Immunosenescence, Graduate School of Medicine, Kyoto University, Shogoin-Kawahara-cho 53, Kyoto, Japan
[2]Department of Immunology and Cell Biology, Graduate School of Medicine, Kyoto University, Kyoto, Japan
[3]Department of Pathology and Biology of Disease, Graduate School of Medicine, Kyoto University, Kyoto, Japan
[4]Division of Host Defense, Medical Institute of Bioregulation, Kyusyu University, Fukuoka, Japan
[5]Department of Immunology, Juntendo University School of Medicine, Tokyo, Japan
[6]Division of Molecular Biology, Research Institute for Biological Science (RIBS), Tokyo University of Science, Chiba, Japan
[7]Medical Innovation Center, Graduate School of Medicine, Kyoto University, Kyoto, Japan
[8]Lead contact
*Correspondence: fukushima.yuji.4x@kyoto-u.ac.jp (Y.F.), hattori.masakazu.8a@kyoto-u.ac.jp (M.H.)
https://doi.org/10.1016/j.celrep.2022.111373

SUMMARY

With age, senescence-associated (SA) CD4^{+} T cells that are refractory to T cell receptor (TCR) stimulation are increased along with spontaneous germinal center (Spt-GC) development prone to autoantibody production. We demonstrate that CD153 and its receptor CD30 are expressed in SA-T and Spt-GC B cells, respectively, and deficiency of either CD153 or CD30 results in the compromised increase of both cell types. CD153 engagement on SA-T cells upon TCR stimulation causes association of CD153 with the TCR/CD3 complex and restores TCR signaling, whereas CD30 engagement on GC B cells induces their expansion. Administration of an anti-CD153 antibody blocking the interaction with CD30 suppresses the increase in both SA-T and Spt-GC B cells with age and ameliorates lupus in lupus-prone mice. These results suggest that the molecular interaction of CD153 and CD30 plays a central role in the reciprocal activation of SA-T and Spt-GC B cells, leading to immunosenescent phenotypes and autoimmunity.
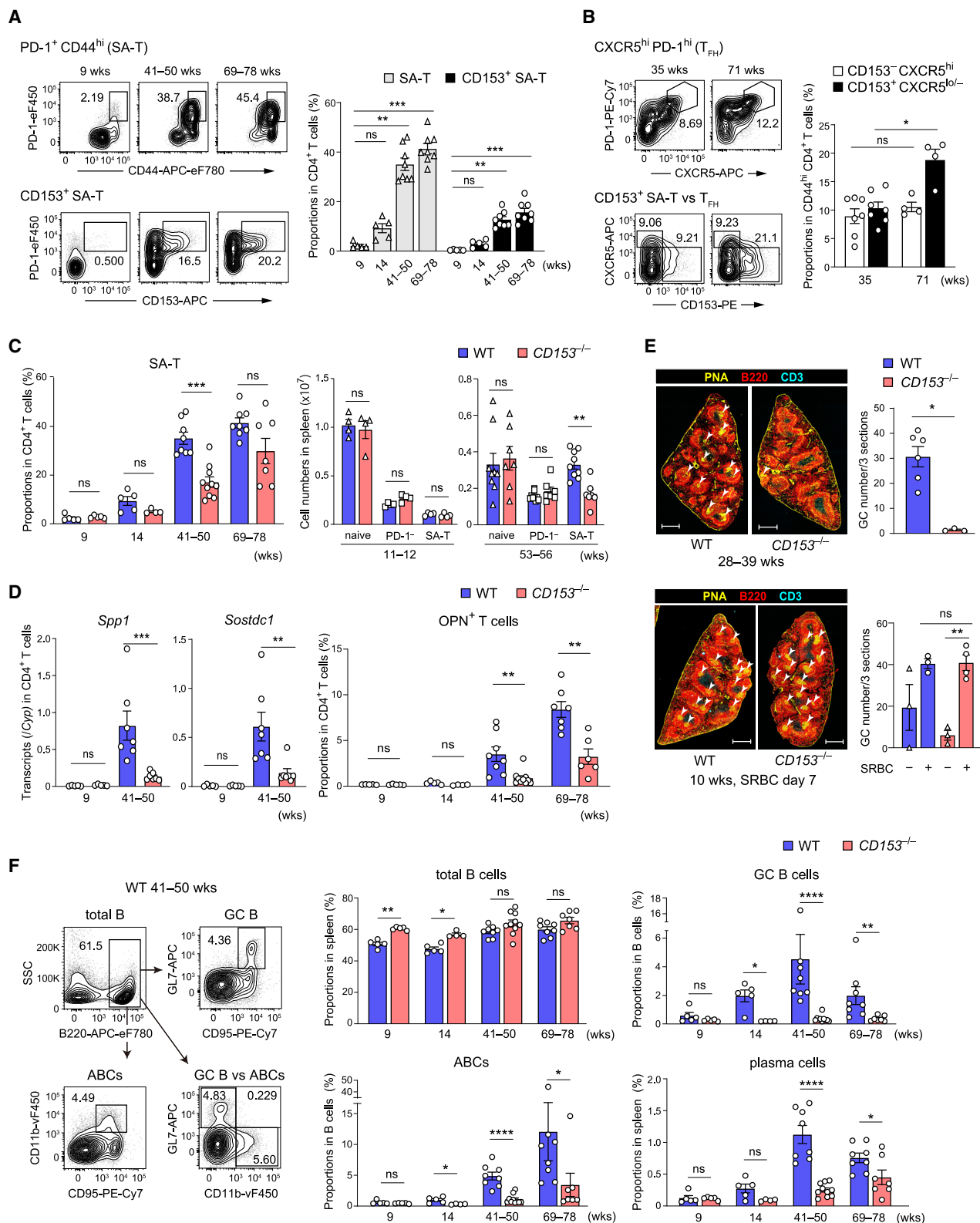
INTRODUCTION

The acquired immune system can show progressive dysfunction with age, including compromised resistance to infection and possibly cancer as well as an increased propensity for chronic inflammation and systemic autoimmunity (Goronzy and Weyand, 2019; Mittelbrunn and Kroemer, 2021; Palmer et al., 2018; Yanes et al., 2017). Such age-related changes in immune function, referred to as immunosenescence, are associated with an increase and accumulation of specific lymphocyte subpopulations in both T and B cell compartments. CD11b^{+} CD11c^{+} T-bet^{+} B cells, termed age-associated B cells (ABCs), are increased with age; these B cells show vigorous responsiveness to Toll-like receptor 7 (TLR7) ligands, serve as potent antigen-presenting cells (APCs), and may be involved in the production of antinuclear antibodies (ANAs) (Hao et al., 2011; Rubtsov et al., 2011). Spontaneous germinal centers (Spt-GCs) including autoreactive GC B cells may also develop, contributing to systemic autoimmunity (Domeier et al., 2016; Fillatreau et al., 2021; Soni et al., 2014). In the T cell compartment, memory-phenotype CD44^{hi} CD4^{+} T cells constitutively expressing programmed cell death protein-1 (PD-1) and bearing a series of features resembling senescent or exhausted cells are increased and accumu-

lated with age, termed senescence-associated T cells (SA-T cells) (Elyahu et al., 2019; Fukushima et al., 2018; Minato et al., 2020; Shimatani et al., 2009). SA-T cells are defective in the proliferation and production of regular T cell cytokines in response to even optimal T cell receptor (TCR) stimulation but are potentially capable of producing abundant atypical cytokines including pleiotropic osteopontin (OPN), reminiscent of the SA secretory phenotype (Shimatani et al., 2009).

The most prominent age-dependent change in lymphoid tissues is early thymic involution (Sekai et al., 2014), and with age, the maintenance of T cell numbers and repertoire becomes increasingly dependent on the polyclonal homeostatic proliferation (HP) of peripheral naive T cells driven through tonic TCR stimulation via the self-peptide/major histocompatibility complex and homeostatic cytokines (Goronzy and Weyand, 2019; Hamazaki et al., 2016; Nikolich-Žugich, 2014). SA-T cells can be developed in the process of sustained HP of naive CD4^{+} T cells under T-lymphopenic conditions (Sato et al., 2017). Thus, we reported that repeated rounds of slow-rate cell divisions during HP eventually leads to the generation of PD-1^{+} CD44^{hi} CD4^{+} T cells from CD44^{lo} naive CD4^{+} T cells bearing functional and genetic features indistinguishable from SA-T cells, including increased gene expression of cyclin-dependent

A PD-1+ CD44hi (SA-T)

B CXCR5hi PD-1hi (TFH)

C SA-T

D *Spp1* *Sostdc1* OPN+ T cells

E

F WT 41–50 wks

total B cells   GC B cells

ABCs   plasma cells

(legend on next page)

kinase inhibitor 1A, 2B (*Cdkn1a*, *2b*) and proinflammatory cytokines such as secreted phosphoprotein 1 (*Spp1*) encoding OPN (Tahir et al., 2015). These features were particularly prominent in the portion of SA-T cells expressing CD153, a tumor necrosis factor (TNF) superfamily (TNFSF) member. Of note, CD153^{+} SA-T cells are preferentially localized in the follicular region of lymphoid tissues often in association with sizable Spt-GCs (Tahir et al., 2015).

Besides aging, CD153^{+} SA-T cells are also robustly increased in lupus as well as in various chronic inflammatory disorders (Fukushima et al., 2018; Sakamoto et al., 2016; Shirakawa et al., 2016; Tahir et al., 2015; Sato et al., 2022). Various tissue-damaging insults inducing acute inflammation in the kidneys can eventually be cleared in the young but may cause persistent inflammation and progress to chronic kidney disease in the elderly, which is often associated with the development of aggressive tertiary lymphoid tissues (TLTs) containing abundant CD153^{+} SA-T cells and GC-like structures (Sato et al., 2016, 2022). Also, a continuous high-fat diet results in a robust increase in SA-T cells in visceral adipose tissues with chronic fat tissue inflammation and insulin resistance (Fukushima et al., 2018; Shirakawa et al., 2016), which persists for a long time even after reversal to a normal diet (Shirakawa et al., 2017). These results indicate the intimately associated development of CD153^{+} SA-T and Spt-GC B cells; however, the underlying mechanisms remain unknown.

In this study, we propose that the molecular interaction of CD153 and CD30 plays a central role in the activation and expansion of SA-T cells and Spt-GC B cells with age as well as in the pathogenesis of lupus in lupus-prone mice.

RESULTS

Involvement of CD153 in age-dependent increases in SA-T cells, ABCs, and Spt-GCs

In the CD4^{+} T cell population, there was a progressive increase in the proportion of PD-1^{+} CD44^{hi} (SA-) T cells with age, and the development of CD153^{+} SA-T cells became evident in mice at $\geq$50 weeks of age (Figure 1A). Although the PD-1^{+} CD44^{hi} CD4^{+} T cell population includes a minor PD-1^{hi} C-X-C chemokine receptor type 5 (CXCR5)[hi] CD153^{−} cell population corresponding to follicular helper T (T[FH]) cells (Vinuesa et al., 2016), CD153^{+} SA-T cells barely exhibited high CXCR5 expression

(Figure 1B). Also, unlike CD153^{+} (CXCR5^{−/lo}) SA-T cells, the CD153^{−} CXCR5^{hi} T[FH] cells showed little further increase in the later stages (Figure 1B). Among all leucocytes in aged mice, the expression of CD153 was confined to a portion of SA-T cells (Figure S1A); therefore, we addressed the functional involvement of CD153 in the development of SA-T cells with the use of *CD153*^{−/−} C57BL/6 (B6) mice. We found that age-dependent increases in the proportion of SA-T cells in the CD4^{+} T cell population was compromised and delayed in *CD153*^{−/−} mice (Figure 1C). Although the proportion of SA-T cells tended to vary as the mice aged, the actual SA-T cell numbers in the spleen were significantly and selectively decreased in *CD153*^{−/−} compared with wild-type (WT) mice at >50 weeks (Figure 1C). Next, we examined the expression of genes characteristic of SA-T cells, which were most prominent in the CD153^{+} fraction (Elyahu et al., 2019; Sakamoto et al., 2016; Sato et al., 2017). While the expression of *Spp1* and sclerostin domain-containing protein 1 (*Sostdc1*) in CD4^{+} T cells was markedly increased in aged WT mice as anticipated, CD4^{+} T cells from aged *CD153*^{−/−} mice showed significantly reduced expression of these transcripts (Figure 1D). Consistently, CD4^{+} T cells capable of rapidly expressing OPN upon treatment with phorbol 12-myristate 13-acetate (PMA) and ionomycin (OPN^{+} T cells) were also significantly reduced in aged *CD153*^{−/−} mice compared with age-matched WT mice (Figure 1D). Furthermore, while aged WT mice developed abundant Spt-GCs in the spleen, age-matched *CD153*^{−/−} mice rarely showed such Spt-GCs (Figure 1E). By contrast, *CD153*^{−/−} mice developed robust GC reactions in response to sheep red blood cell (SRBC) immunization comparable to WT mice (Figure 1E). Immunoglobulin G (IgG) antibody (Ab) production to nonylphenol-ovalbumin (NP-OVA) immunization was partially reduced at the peak but became comparable in a later phase (Figure S1B), suggesting that the role of CD153, if any, might not be essential. Fluorescence-activated cell sorting (FACS) analysis confirmed the remarkable decrease of GC B cells (CD95^{+} GL7^{+} CD11b^{−} B220^{+}) as well as ABCs (CD95^{+} GL7^{−} CD11b^{+} B220^{+}) and plasma cells (CD138^{+}) in aged *CD153*^{−/−} mice, although the total B cell population was unaffected (Figure 1F). Accordingly, the development of hyperglobulinemia, particularly of IgG2c and IgG2b classes, as well as anti-DNA Abs was significantly compromised in aged *CD153*^{−/−} compared with WT mice (Figure S1C). These results indicate that CD153 plays a significant functional role in the

---

Figure 1. Involvement of CD153 in age-dependent increases in CD153^{+} SA-T cells, ABCs, and Spt-GCs

(A) Representative flow cytometry profiles of SA-T cells (PD-1^{+} CD44^{hi}) and CD153^{+} SA-T cells and their frequencies in splenic CD4^{+} T cells from WT mice (n = 5–8 mice/group).

(B) Flow cytometry profiles of T[FH] cells (CD153^{−} CXCR5^{hi} PD-1^{hi}) and CD153^{+} SA-T cells (CD153^{+} CXCR5^{−/lo}) in the CD44^{hi} CD4^{+} T cell gate of spleen cells from WT mice (n = 4–7 mice/group).

(C) Frequencies of SA-T cells in a CD4^{+} T cell population and absolute cell numbers in spleens from WT and *CD153*^{−/−} mice (n = 4–10 mice/group). naive, CD44^{lo} CD62L^{+}; PD-1^{−}, PD-1^{−} CD44^{hi}; SA-T, PD-1^{+} CD44^{hi}.

(D) Expression of *Spp1* and *Sostdc1* transcripts and frequencies of OPN^{+} cells in splenic CD4^{+} T cells from WT and *CD153*^{−/−} mice (n = 5–10 mice/group).

(E) Spleens from WT and *CD153*^{−/−} mice and those immunized with SRBCs were immunostained with indicated markers. Bars, 500 μm; arrowheads, PNA^{+} GCs. GC numbers are shown (n = 3–6 mice/group).

(F) Representative flow cytometry profiles of GC B cells (GL7^{+} CD95^{+} CD11b^{−}) and ABCs (GL7^{−} CD95^{+} CD11b^{+}) in a splenic B cell population from aged WT mice (left). Frequencies of total B cells, GC B cells, ABCs, and plasma cells (CD138^{+}) in spleen cells from WT and *CD153*^{−/−} mice (right; n = 4–10 mice/group).

Data represent the mean ± standard error of the mean (SEM). ns, not significant; *p < 0.05, **p < 0.01, ***p < 0.001, and ****p < 0.0001 by Kruskal-Wallis test with Dunn's multiple comparison test (A), two-sided Mann-Whitney U test (B–D, E; upper, F), one-way analysis of variance (ANOVA) with Šidák's multiple comparison test (E; lower). Please also see Figure S1.

age-dependent increase in SA-T cells as well as Spt-GC B cells and ABCs.

CD30 deficiency results in similar phenotypes as *CD153*⁻/⁻ mice with age

FACS analyses indicated that the CD30 (CD153 receptor) was weakly yet detectably expressed on the cell surface only in portions of Spt-GC B cells and ABCs in addition to SA-T cells among leukocytes in elderly mice (Figure 2A). Since our previous report indicated that SA-T cells rarely develop in B cell-deficient (μMT) mice (Tahir et al., 2015), we investigated the involvement of CD30 in the development of SA-T cells. Elderly *CD30*⁻/⁻ mice also showed a significantly compromised increase in SA-T cells as well as OPN⁺ CD4⁺ T cells compared with age-matched WT mice (Figure 2B). Consistently, CD4⁺ T cells in elderly *CD30*⁻/⁻ mice exhibited remarkably reduced transcripts of *Tnfsf8* (*Cd153*) as well as *Spp1*, *Sostdc1*, and *Cdkn2b*, close to the levels in CD4⁺ T cells from young 11-week-old WT mice (Figure 2B). Furthermore, elderly *CD30*⁻/⁻ mice also showed markedly decreased Spt-GC B cells and ABCs compared with age-matched WT mice, again with no change in total B cells (Figure 2C). We examined the role of CD30 in GC-B cell development *in vitro* using culture conditions recapitulating GC reactions (Nojima et al., 2011). Isolated splenic B cells were cultured together with 3T3 cells expressing B cell activating factor (BAFF) and CD40 ligand (CD40L), 40LB, or 40LB cells additionally expressing CD153 (CD153/40LB) in the presence of interleukin 4 (IL-4) (Figure S2). The expression of CD30 was strongly induced on B cells in the culture, and the yield of *in vitro*-induced GC B (iGB) cells was remarkably increased in the presence of CD153/40LB cells compared with 40LB cells, with enhanced expression of B cell lymphoma-related genes (*B cell lymphoma 2 [Bcl2]*, *B cell lymphoma-extra large [BclXL]*) (Figure 2D). These results suggest that CD30 also plays an important role in the development of both SA-T cells and Spt-GCs with age.

CD153 engagement restores TCR signaling in CD153⁺ SA-T cells

We addressed how CD153 might affect the function of CD153⁺ SA-T cells. To this end, we prepared primary CD153⁺ SA-T cells (PD-1⁺ Lag3⁺ CD25⁻ CD121b⁻ CD44^hi CD4⁺) enriched to about 75% purity from aged mouse spleen cells without using anti-CD153 Ab (Figures S3A and S3B) and cultured them in the absence or presence of solid-phase anti-CD153 Ab (RM153) with or without TCR stimulation. The enriched CD153⁺ SA-T cells showed no Ki67 expression, a marker of cell cycle progression, in response to anti-CD3 Ab with only minimal induction in the additional presence of anti-CD28 Ab, whereas PD-1⁻ (CD25⁻) CD44^hi CD4⁺ T cells from the same mice exhibited maximal proliferation in response to even anti-CD3 Ab alone (Figure 3A). However, CD153⁺ SA-T cells cultured in the presence of RM153 together with anti-CD3 + CD28 Abs exhibited significant Ki67 expression, if not fully comparable to PD-1⁻ CD25⁻ CD44^hi CD4⁺ T cells (Figure 3A). RM153 alone or RM153 with anti-CD3 Ab in the absence of anti-CD28 Ab induced negligible responses in CD153⁺ SA-T cells (Figure 3A). RM153 also induced remarkable enhancement in the production of OPN and IL-4 in response to anti-CD3 + CD28 Abs. The production of other typical T cell

cytokines including interferon gamma (IFN-γ), TNF-α, IL-2, and C-C motif chemokine ligand 3 (CCL3) was also enhanced, but the levels remained much lower than those in PD-1⁻ CD25⁻ CD44^hi CD4⁺ T cells (Figure 3B). These results were confirmed at the transcript level (Figure S3C). RM153 caused slight enhancement of IFN-γ, TNF-α, and CCL3, and negligible OPN production in PD-1⁻ CD25⁻ CD44^hi CD4⁺ T cells (Figure 3B), likely due to transient CD153 expression upon TCR stimulation (Shimozato et al., 1999). Comparative RNA sequencing analyses indicated that CD153⁺ SA-T cells stimulated with anti-CD3 + CD28 Abs in the presence of RM153 for 16 h showed significantly increased expression of some 20 genes compared with those cultured with anti-CD3 + CD28 Abs and control IgG (Figure 3C). Kinetic analyses with quantitative PCR (qPCR) revealed that RM153 caused a significant increase in the gene expression of IFN regulatory factor 4 (*Irf4*) followed by *c-Myc*, activating transcription factor 3 (*Atf3*), and T-box transcription factor 21 (*Tbx21*) in the TCR-stimulated CD153⁺ SA-T cells, although the expression of these transcription factor (TF) genes was barely induced in the presence of control IgG (Figure 3C). By contrast, whereas the expression of *Cdkn2b* and *Cdkn1a* was increased in CD153⁺ SA-T cells following TCR stimulation, the effects tended to be less robust in the presence of RM153 (Figure 3C). Despite the defective TCR response, CD153⁺ SA-T cells showed markedly enhanced survival *in vitro* in response to homeostatic cytokines such as IL-7 and IL-15 (Figure S3D); however, the effects of cytokines were not affected by the presence of RM153 (Figure S3E). These results indicate that CD153 engagement concomitant with optimal TCR stimulation significantly restores TCR signaling in CD153⁺ SA-T cells, leading to the proliferation and cytokine production of a specific profile.

CD153 engagement on TCR stimulation causes *cis* association of CD153 with TCR/CD3 and hinders internalization of the TCR complex, enhancing TCR signaling

To address the mechanisms underlying CD153-mediated restoration of TCR responsiveness in CD153⁺ SA-T cells, we generated a CD4⁺ T cell line, EL4, stably expressing CD153-Clover fusion protein (CD153Clov/EL4) with unchanged expression levels of TCR/CD3 and CD28 (Figure S4A). CD153Clov/EL4 cells tended to produce less IL-2 than parental EL4 cells in response to anti-CD3 + CD28 Abs, but the response was significantly enhanced with the addition of RM153, with EL4 cells being unaffected (Figure 4A). Quite unexpectedly, CD153 co-immunoprecipitated (IP'd) with all of the CD3 chains (γ, δ, ε, and ζ) as well as Fc receptor gamma (FcRγ), which may replace CD3ζ (Katsuyama et al., 2018), but not with TCR, CD4, or CD28, in CD153Clov/EL4 cells without any stimulation (Figure 4B). Cotransfection experiments of *Cd153* and individual *Cd3* components or *Fcrg* in human kidney 293T cells confirmed that CD153 was capable of associating with individual CD3 chains and FcRγ even in the absence of TCR (Figure 4B). Stimulation of CD153Clov/EL4 cells with anti-CD3 + CD28 Abs did not result in the detectable association of CD153 and TCR. However, additional stimulation with RM153 caused the association of CD153 with TCR, which took place within 5 min and stably increased thereafter at least until 60 min (Figure 4C). Normally, TCR
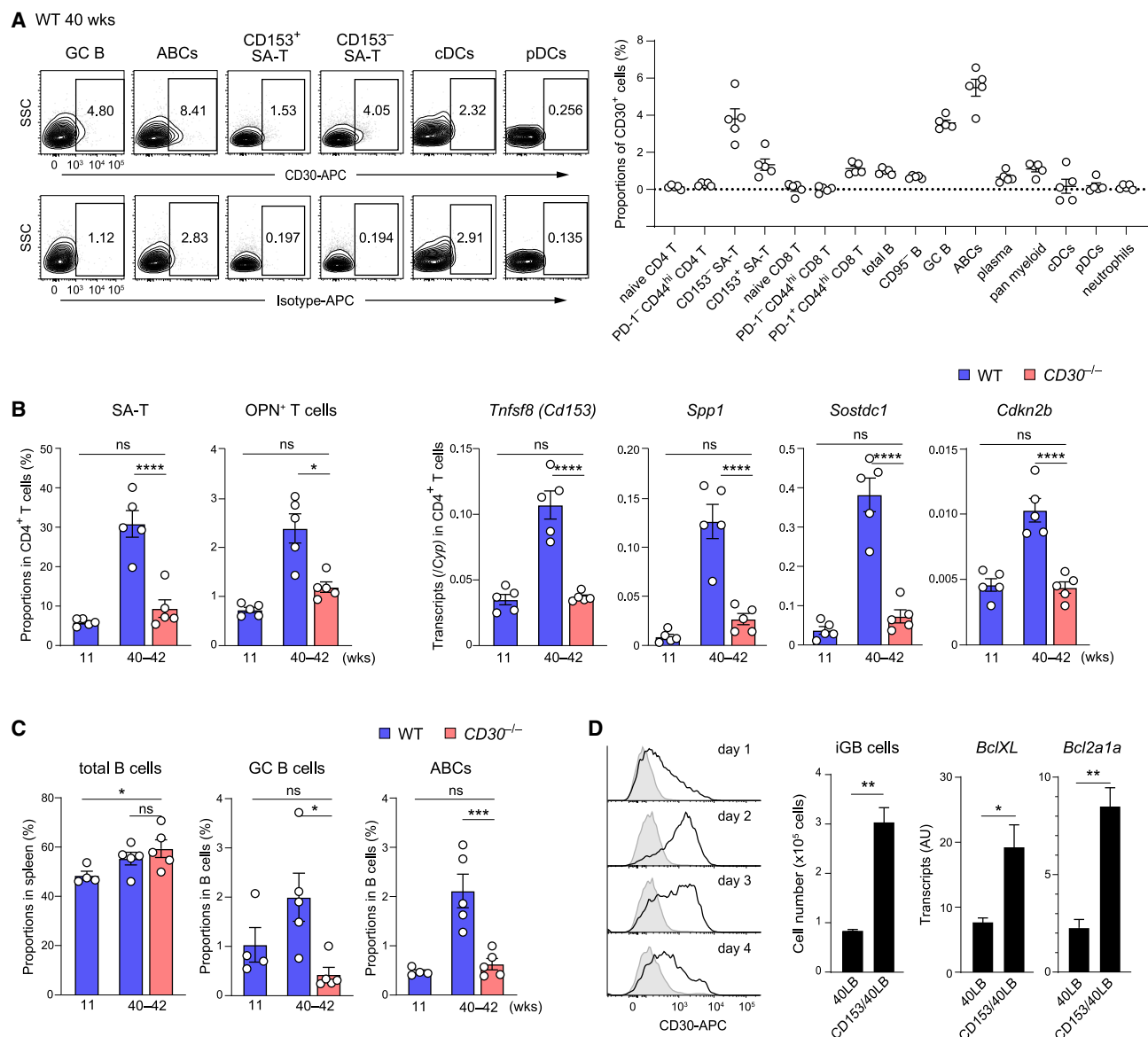
Figure 2. CD30 deficiency results in similar phenotypes as *CD153⁻/⁻* mice with age

(A) Surface expression of CD30 in various populations of splenic cells from WT B6 mice at 40 weeks of age. Representative flow cytometry profiles and frequencies of CD30⁺ cells are shown (n = 5 mice). The cell populations are defined elsewhere in this article or otherwise as follows: CD8⁺ T cells (CD4⁻ CD3ε⁺), pan myeloid cells (CD11b⁺), conventional dendritic cells (cDCs; CD11cʰⁱ CD11b⁺), plasmacytoid DCs (pDCs; Siglec-h⁺ CD11b⁻), and neutrophils (Gr-1ʰⁱ CD11bʰⁱ).

(B and C) Frequencies of the indicated CD4⁺ T cell subpopulations, expression of the transcripts in CD4⁺ T cells (B), as well as frequencies of the total and indicated B cell subpopulations (C) in WT and *CD30⁻/⁻* mice are shown (n = 4 or 5 mice/group).

(D) Representative flow cytometry histograms of CD30 expression on iGB cells at the indicated days in the culture. The yields of iGB cells and expression of *BclXL* and *Bcl2a1a* transcripts in the presence of 40LB or CD153⁺ 40LB feeder cells are shown (day 3; n = 4).

Data represent the mean ± SEM. ns, not significant; *p < 0.05, **p < 0.01, ***p < 0.001, and ****p < 0.0001 by one-way ANOVA with Dunnett's multiple comparison test or Kruskal-Wallis test with Dunn's multiple comparison test (B and C) and two-sided paired Student's t test (D). Please also see Figure S2.

stimulation results in the rapid decrease of the cell surface TCR/ CD3 complex due to endocytosis followed by degradation (Valitutti et al., 1995). Immunostaining analyses showed a remarkable increase in the clusters of TCR complex following anti-CD3 + CD28 Ab stimulation, and it was confirmed that the TCR clusters

had been internalized (Figure 4D) using the Cellpose cell boundary determination method (Stringer et al., 2021). However, in the presence of RM153, such internalized TCR clusters were significantly diminished compared with the control IgG (Figure 4D), and CD153 associated with the TCR complex remained at the
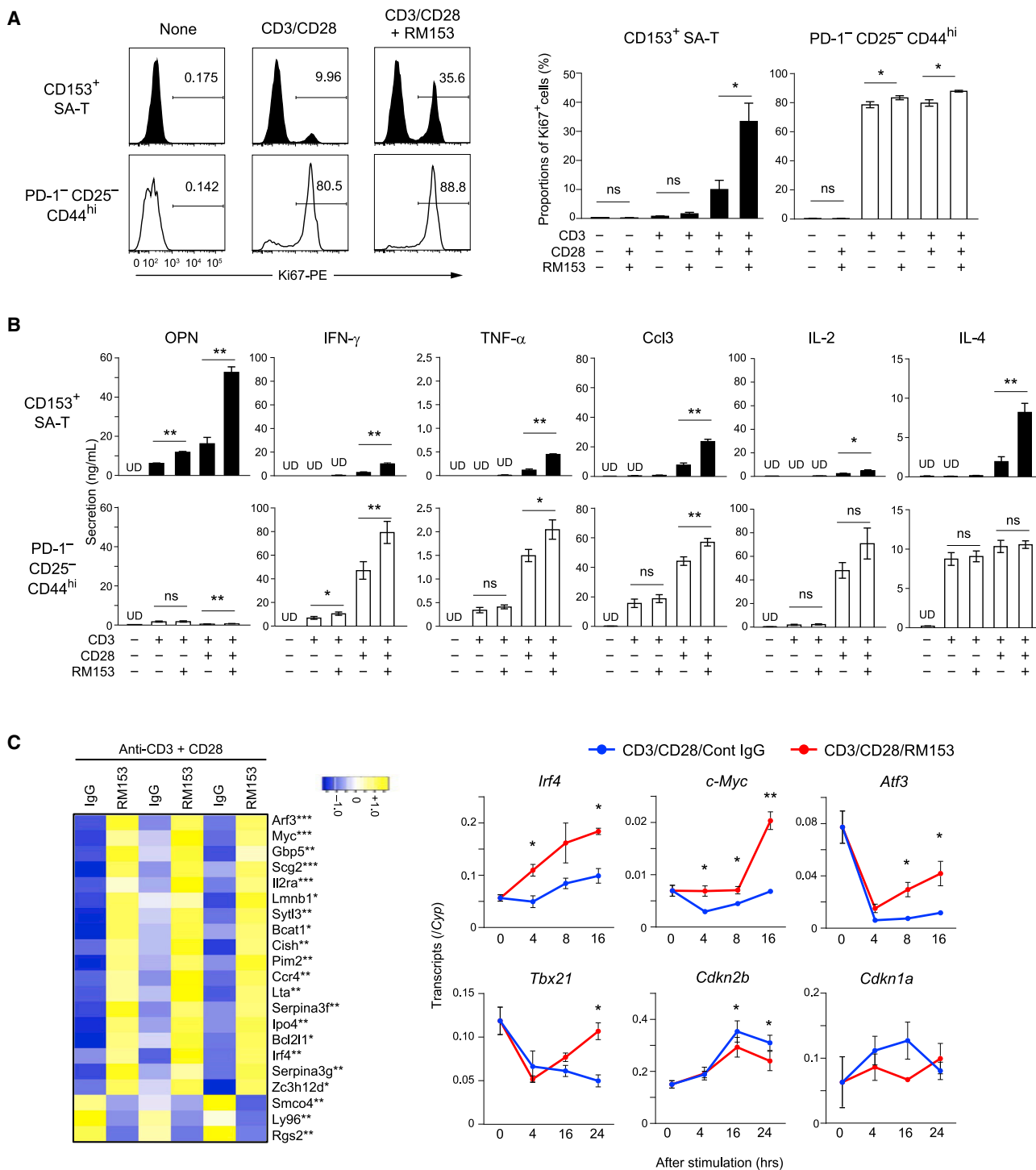
Figure 3. CD153 engagement restores TCR signaling in CD153+ SA-T cells

(A and B) CD153+ SA-T cells and PD-1− CD25− CD44hi cells were enriched from aged WT B6 mice, and stimulated with anti-CD3 and/or anti-CD28 Abs in the presence or absence of RM153 for 3 days.

(A) Representative flow cytometry histograms of Ki67 expression and the percentages of Ki67+ cells in the presence of the indicated combinations of Abs (n = 3).

(B) Secretion of cytokines and chemokines in the culture supernatants (n = 3). UD, undetected.

(legend continued on next page)

cell surface, with CD153 being rarely detectable in the internalized TCR clusters (Figure 4E). FACS analyses using primary CD153⁺ SA-T cells confirmed that the reduction of the cell surface TCR/CD3 complex following TCR stimulation was significantly delayed in the presence of RM153 (Figure S4B). In accordance with these findings, co-engagement of CD153 caused remarkably enhanced phosphorylation of the proximal zeta chain of T cell receptor-associated protein kinase 70 (ZAP70) via TCR stimulation (Figure 4E). Extracellular signal-regulated kinase (ERK) activation was also markedly enhanced and lasted as long as 90 min in the presence of RM153, although the activation of p38 mitogen-activated protein kinase (MAPK) and c-Jun N-terminal kinase (JNK) was unaffected (Figures 4E and S4C). To avoid the possible effects of anti-CD3ε Ab on CD3ε pre-associated with CD153, we repeated the experiments using anti-TCRβ Ab instead of anti-CD3ε Ab for stimulation, and we obtained almost identical results (Figure S4D). Primary SA-T cells showed increased *Fcrg* expression compared with naive CD4⁺ T cells (Figure S4E). Furthermore, RM153 could enhance the phosphorylation of FcRγ in addition to CD3ζ in CD153Clov/ EL4 cells (Figure S4E). Thus, additional signaling downstream of FcRγ may be involved in the selective TCR-mediated activation of ERK among MAPKs. The enhancing effect of RM153 on TCR-mediated ERK activation was similarly observed in EL4 cells expressing CD153 with its entire cytoplasmic domain (N-terminal 44 residues) replaced by Clover, CD153ΔCD, strongly arguing against the involvement of possible signaling mediated via CD153 alone (Figure S4F). Collectively, these results suggest that optimal TCR stimulation with concomitant engagement of CD153 causes *cis* association of CD153 with TCR/CD3 on the cell surface via CD3 components to hinder endocytosis of the engaged TCR complex, allowing effective TCR signaling in CD153⁺ SA-T cells.

Ab-mediated blockade of CD153 engagement suppresses the development of SA-T and GC B cells *in vivo*

Based on the results indicating the crucial involvement of CD153 and CD30 in the development of SA-T and Spt-GC B cells, we attempted the blockade of CD153/CD30 interaction *in vivo*. To this end, we generated a mouse anti-CD153 monoclonal Ab, termed 17D, which strongly inhibited the binding of CD153⁺ cells to the CD30-Ig fusion protein (EC₅₀, about 10 μg/mL) with minimal complement-dependent cytotoxicity in CD153⁺ cells (Figure 5A). Epitope mapping analyses suggested that 17D recognized a conformational epitope partly overlapping the putative CD30-binding region (Figures 5B, S5A, and S5B). First, we examined the short-term effects of 17D administration on SA-T cells induced by a TLR7 agonist (R848). R848 administration for 1 month caused a marked increase in SA-T cells and GC B cells in young 9- to 10-week-old B6 mice (Figure 5C) as

previously reported (Sakamoto et al., 2016). Although subsequent treatment with 17D for 1 week did not affect the proportions of SA-T and GC B cells (Figure 5C), Ki67 expression in the SA-T cell population was significantly decreased by 17D administration compared with that in the control IgG-treated group, with only marginal effects, if any, on PD-1⁻ CD44ʰⁱ CD4⁺ T cells (Figure 5C), suggesting that 17D preferentially inhibited the cell cycle progression of SA-T cells without directly affecting their viability. Next, to examine the effects on the age-dependent increase in SA-T cells, we administered 17D or control IgG to elderly B6 mice aged about 40 weeks for 1 month. We found a significantly compromised increase in SA-T cells in the 17D-treated group, and accordingly, OPN production in CD4⁺ T cells was diminished compared with the control group (Figure 5D). These 17D-treated mice also showed significantly reduced development of Spt-GC B cells, although the decrease in ABCs was not statistically significant (Figure 5D). Of note, 17D treatment did not affect the IgG Ab response against NP-OVA immunization (Figure S5C). These results suggest that the CD153/CD30 interaction plays an important role in the reciprocal development of SA-T and Spt-GC B cells with age.

Amelioration of lupus development and progression with 17D administration to lupus-prone mice

Given the robust and premature increase in SA-T cells in association with the massive development of Spt-GCs in lupus-prone mice (Sakamoto et al., 2016; Tahir et al., 2015), we investigated the effects of 17D administration on lupus. First, we initiated the administration of 17D or control IgG to female (NZB x NZW) F₁ (BWF₁) mice at 16 weeks of age, when no clinical evidence of lupus was yet detectable, for 4 months (Set 1; Figure 6A). In the control group, serum anti-double-stranded DNA (dsDNA) Ab titers were increased beginning from about 24 weeks of age and robustly thereafter. However, 17D-treated mice showed only a minimal increase in anti-dsDNA Ab titers until 32 weeks of age (Figure 6B). At the end of the experiment at 32 weeks of age, control BWF₁ mice showed a remarkable increase in the proportions of SA-T and GC-B cells as well as Spt-GC numbers, but the development of both cell types was significantly compromised in 17D-treated BWF₁ mice; the proportions of PD-1ʰⁱ CXCR5ʰⁱ T_FH cells were unaffected by 17D administration (Figure 6C). Importantly, 17D-treated mice showed remarkably reduced glomerular IgG deposition with little histological evidence of nephritis, whereas 60% of control mice developed overt glomerulonephritis (Figure 6D). Administration of RM153 with much lower blocking activity of CD153/CD30 interaction than 17D showed little effects on anti-dsDNA Ab titers and Spt-GC B cells (Figures S6A and S6B). Then we examined the delayed initiation of 17D treatment at 28 weeks of age, when the BWF₁ mice had already developed high titers of anti-dsDNA Ab, as a therapy model (Set 2; Figure 6A). In 17D-treated BWF₁ mice, a further

---

(C) Enriched CD153⁺ SA-T cells were stimulated with anti-CD3 + CD28 Abs in the presence of RM153 or control IgG. Bulk RNA sequencing analyses at 16 h after stimulation (left; n = 3 for each). Representative genes with increased (yellow) and decreased (blue) expression at more than 1.6-fold are shown. *Benjamini-Hochberg-adjusted p < 0.1, **p < 0.05, ***p < 0.01. qPCR analyses at the indicated intervals for the indicated genes (right; n = 3–4 for each gene).
Data indicate the mean ± SEM. ns, not significant; *p < 0.05 and **p < 0.01 by two-sided paired Student's t test (between samples at the same time point). Please also see Figure S3.
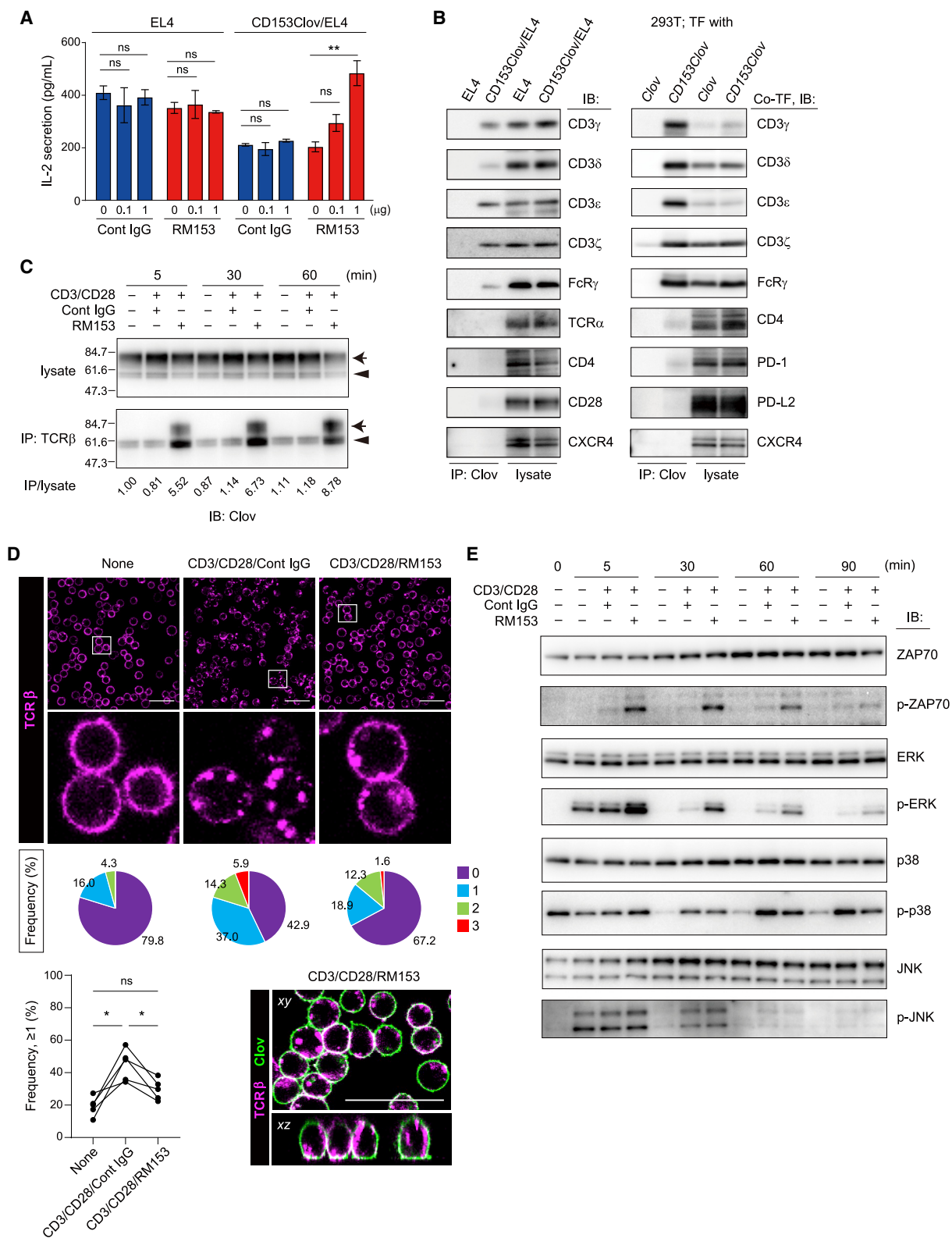
(legend on next page)

increase in anti-dsDNA titers tended to be halted (Figure 6E), and more importantly, the development of overt proteinuria was compromised and overall survival rate was significantly improved (Figures 6F and 6G). The effects were nearly comparable to those of the DNA synthesis inhibitor mycophenolate mofetil. These results suggest that the early robust expansion of SA-T and Spt-GC B cells in genetically lupus-prone mice is also caused by the reciprocal CD153/CD30 interaction between the two cell populations (Figure S6C), resulting in overt systemic autoimmune disease.

DISCUSSION

A progressive increase in SA-T cells with profound refractoriness even to optimal TCR stimulation may underlie the dysfunction of the overall CD4$^+$ T cell population in infection and malignancy with age (Shimatani et al., 2009; Minato et al., 2020). Rather paradoxically, however, the increase in SA-T cells also tends to be associated with the spontaneous development of GCs in lymphoid tissues leading to hyperglobulinemia often with autoantibody production (Sakamoto et al., 2016; Tahir et al., 2015). In this study, we investigated the mechanisms underlying the apparently associated increase in SA-T cells and Spt-GC B cells with age.

We found that the age-dependent increase in SA-T cells was significantly compromised and delayed in $CD153^{-/-}$ mice. CD153 expression was confined to a portion of SA-T cells among all leukocytes in aged mice, strongly suggesting the direct role of CD153 in the increase in CD153$^+$ SA-T cells with age. In addition, $CD153^{-/-}$ mice also showed the remarkable suppression of age-dependent development of Spt-GCs as well as ABCs, resulting in the abrogation of hyperglobulinemia and ANA production in aged mice. CD30, a receptor for CD153, was selectively expressed on minor portions of Spt-GC B cells and ABCs in aged mice, and aged $CD30^{-/-}$ mice also showed a remarkable decrease of Spt-GCs along with SA-T cells with age. CD153 ligation of the CD30 receptor induces TNF receptor-associated factor-mediated signaling such as nuclear factor kappa B activation (Xie, 2013), and we confirmed that the introduction of CD153$^+$ feeder cells markedly promoted the generation of CD30$^+$ GC B cells using the culture system recapitulating GC B cell development (Nojima et al., 2011).

Considering that SA-T cells are mostly localized in the follicular regions and the development is defective in B cell-deficient μMT mice (Tahir et al., 2015), the results are consistent with the notion that the cognitive CD153/CD30 interaction between CD153$^+$ SA-T cells and CD30$^+$ Spt-GC B cells plays a central role in the reciprocal development of both cell populations. ABCs reside in the T/B cell border or the marginal zone in their trajectory (Rubtsov et al., 2015; Song et al., 2022); it remains to be determined whether ABCs can be involved in Spt-GCs on their activation.

Although CD153$^+$ SA-T cells in aged mice hardly responded to optimal TCR stimulation with anti-CD3 + CD28 Abs, these cells showed significant proliferation and activation in the concomitant presence of anti-CD153 Ab (RM153). RM153 alone failed to activate the CD153$^+$ SA-T cells, and TCR costimulation with anti-CD28Ab was needed for the effects of RM153 to occur. Indeed, TCR stimulation of CD153$^+$ SA-T cells in the presence of RM153 caused the orchestrated induction of TF genes crucial for T cell proliferation and activation, such as *Irf4*, *c-Myc*, *Atf3*, and *Tbx21*, resulting in cell cycle progression and the production of a specific set of cytokines including OPN and IL-4. Thus, these results revealed that CD153$^+$ SA-T cells were not "terminally" exhausted with irreversible dysfunction. CD153$^+$ SA-T cells express high levels of *Cdkn1a* and *Cdkn2b* resembling senescent cells (Tahir et al., 2015), which may be further increased upon TCR stimulation. Also, similarly to human CD4$^+$ T cells in aged individuals (Li et al., 2012), CD153$^+$ SA-T cells show a pronounced decrease in miR-181a targeting certain phosphatase genes with increased expression of several protein tyrosine phosphatase genes (Tahir et al., 2015). These features may contribute to the raised intracellular threshold for TCR signaling and its effects on CD153$^+$ SA-T cells. Nonetheless, the current results suggest that CD153 engagement upon TCR stimulation somehow allows the TCR-mediated signal to surmount the elevated threshold, provided that the optimal signal scaffold is assured by TCR costimulation with the CD28 signal.

In this study, we found that CD153 is capable of being associated with each of the CD3 chains and FcRγ but not with TCR, CD4, or CD28, independent of TCR at the cell surface. While CD153 has a conserved basic residue at the outer end of the putative transmembrane (TM) region, it remains to be seen whether the residue is involved in the association with CD3 akin to TCR. It

Figure 4. CD153 engagement on TCR stimulation causes *cis* association of CD153 with TCR/CD3 and hinders internalization of the TCR complex, enhancing TCR signaling

(A) IL-2 production by EL4 and CD153Clov/EL4 cells stimulated by anti-CD3 + CD28 Abs in the presence of the indicated concentrations of RM153 or control rat IgG for 3 days. Data (mean ± standard deviation [SD] of triplicate samples) are representative of two experiments with similar results. ns, not significant; **p < 0.01 by one-way ANOVA with Dunnett's multiple comparison test.

(B) EL4 and CD153Clov/EL4 cells (left) as well as 293T cells co-transfected (Co-TF) with *Clover* or *CD153-Clovver* and each of the indicated genes (right) were IP'd with anti-Clover Ab followed by immunoblotting (IB) with the indicated Abs.

(C and E) CD153Clov/EL4 cells were stimulated with the indicated combinations of Abs against CD3, CD28, and CD153 for varying durations.

(C) Cell lysates, either straight or following IP with anti-TCRβ Ab, were probed with anti-Clover Ab. Arrows, glycosylated CD153Clov; arrowheads, CD153Clov with little glycosyl modification (overlapping the heavy chain bands of anti-TCRβ Ab when IP'd). Relative IP signal densities normalized to those in straight lysates are shown.

(E) Cell lysates were probed with the indicated Abs.

(D) CD153Clov/EL4 cells pre-stained with anti-TCRβ Ab were stimulated with anti-CD3 + CD28 Abs in the presence of control IgG or RM153 for 30 min and analyzed by confocal microscopy. Frequencies of cells with internalized TCRβ (0, 1, 2, 3, and >3 vesicles within a cell) are determined. Representative data (upper) and repeated measurements (lower left; n = 5) as well as localization of TCRβ and CD153Clov (lower right) are shown. Scale bar, 40 μm; boxes in top panels, areas shown at higher magnification. ns, not significant; *p < 0.05 by one-way ANOVA with Tukey's multiple comparison test. Please also see Figure S4.
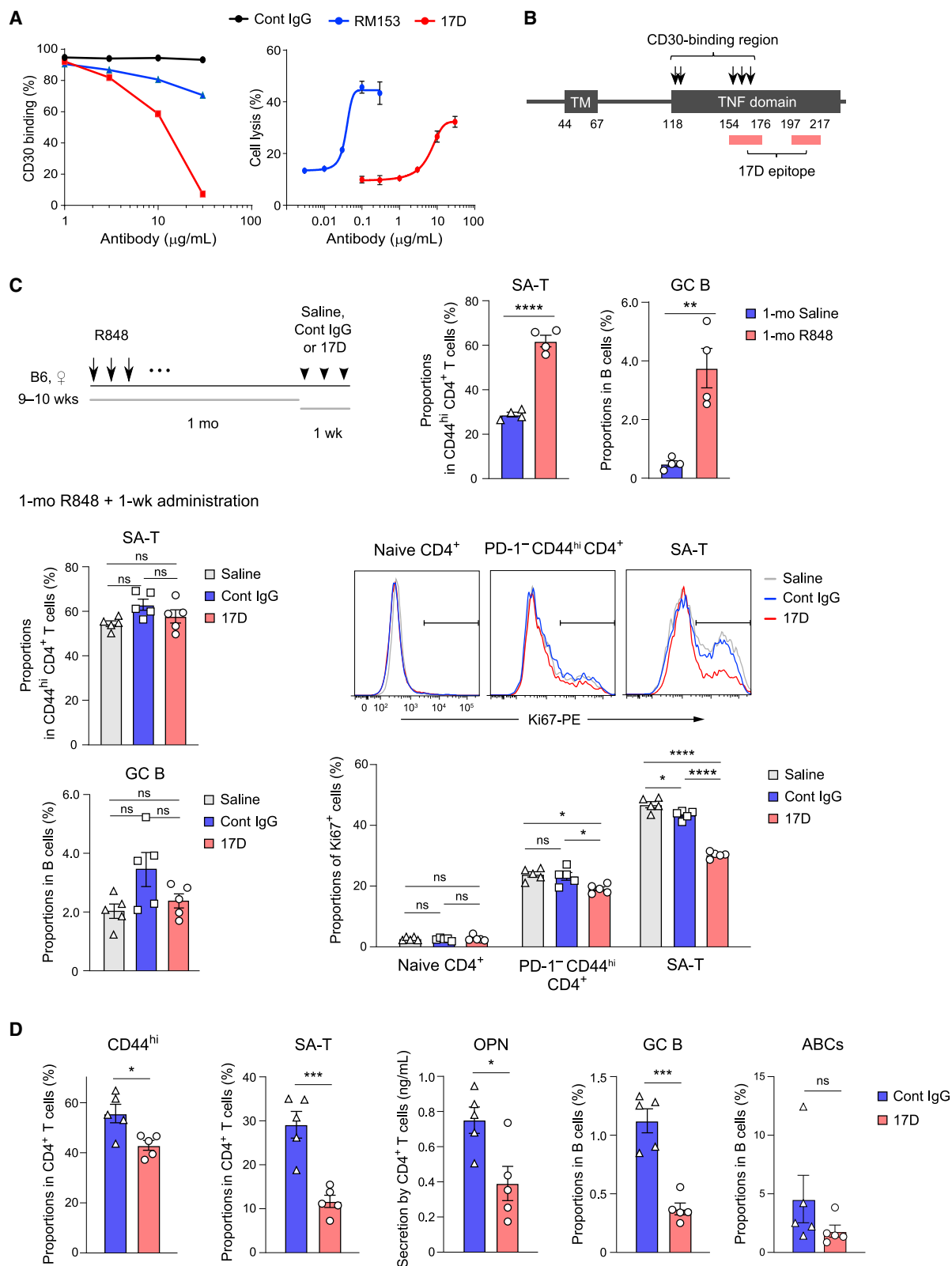
(legend on next page)

is also unknown whether CD153, which normally forms a trimer at the cell surface (Hargreaves and Al-Shamkhani, 2002), is associated with CD3 chains at any ordered stoichiometry. Furthermore, the stimulation of CD153Clov/EL4 cells with anti-CD3 (or anti-TCRβ) + anti-CD28 Abs in the presence of RM153 resulted in the association of CD153 with the TCR/CD3 complex, which occurred rapidly in 5 min and was sustained at least until 60 min. Immunostaining analyses showed that the association of CD153 and the TCR/CD3 complex at the cell surface resulted in the significant inhibition of TCR complex endocytosis following TCR stimulation, which otherwise occurred rapidly followed by degradation (Liu et al., 2000). Among the CD3 chains, CD3ζ has a distinct traffic independent of the remaining CD3 components with a shorter half-life (Ono et al., 1995) and may play an important role in regulating the integrity and stability of the TCR/CD3 complex (Alcover et al., 2018). It is suggested that endocytosis of the TCR/CD3 upon TCR stimulation is initiated by the dissociation of CD3ζ from the TCR/CD3 complex, exposing endocytic motives in other components of the TCR complex (D'Oro et al., 2002). Thus, it is possible that the association of CD153 with the TCR/CD3 complex, particularly via CD3ζ (or FcRγ), hinders TCR complex endocytosis upon TCR stimulation, allowing their prolonged sustenance at the plasma membrane. Supporting this notion, TCR/CD3 associated with CD153 was confined to the cell surface throughout the stimulation periods. Accordingly, CD153 engagement upon TCR stimulation caused markedly enhanced and prolonged phosphorylation of ZAP70 as well as downstream ERK activation; notably, negligible enhancement of p38MAPK or JNK was seen. Distinct MAPKs can be activated independently of each other via association with distinct molecules within the ZAP70 signalosomes, and the dominant MAPK types may vary depending on the TCR signal strength or the type and status of T cells (Daniels et al., 2006; Adachi and Davis, 2011). A portion of the TCR complex in CD153+ SA-T cells seems to include FcRγ in place of CD3ζ, as reported in T cells from patients with systemic lupus erythematosus (Enyedy et al., 2001; Liossis et al., 1998), and the involvement of FcRγ-Syk signaling may underlie the biased MAPK signaling and remains to be investigated. The cognitive interaction of CD153 with CD30 may deliver a "reverse signal" in certain CD153-expressing cells (Su et al., 2004; Sun et al., 2010; Wiley et al., 1996), but RM153 was fully capable of restoring the TCR signaling in CD153ΔCD-expressing T cells. This study underscores the direct molecular association of a TNFSF member with the TCR/CD3 complex to augment TCR-mediated signaling.

Administration of an anti-CD153 Ab, 17D, capable of efficiently blocking the engagement of CD153 with CD30, significantly suppressed the increase in SA-T and Spt-GC B cells in aged mice and ameliorated the development and progression of lupus in female BWF1 mice with significant improvement of overall survival. The effects of 17D Ab were suggested to be due to the efficient blockade of CD153 engagement with CD30, because another anti-CD153 Ab with weaker blocking activity was less effective in lupus. Administration of 17D was effective in both prophylactic and therapeutic protocols in female BWF1 mice. While the lineage relationship between Spt-GC B cells and ABCs remains to be investigated, both B cell subsets seem to share potent APC activity as well as a propensity for autoantibody production (Rubtsov et al., 2011; Soni et al., 2014); thus, it seems likely that these B cells may serve as self-antigens such as nuclear components to SA-T cells in a context similar to HP. Although CD153+ SA-T cells are refractory to antigens via regular professional APCs without CD30 expression such as dendritic cells, these T cells may be efficiently activated with the cognitive interaction with CD30+ B cell subsets via constitutively expressed CD153, which in turn are induced to proliferate and differentiate via CD30 signaling, thereby forming an amplifying circle of mutual activation and expansion. Cytokines such as OPN and IL-4 abundantly secreted from such activated CD153+ SA-T cells may also contribute to the promotion of GC B cell survival and differentiation as well as tissue inflammation (Domeier et al., 2016; Sakamoto et al., 2016). Although CD153 may be transiently induced in activated T_FH cells and enhance the B cell helper effects, the role of CD153 in CD153+ SA-T cells is clearly distinct from this and initiates their progressive expansion along with CD30+ B cells.

A prominent feature of age-related diseases is chronic inflammation in a variety of tissues (Ferrucci and Fabbri, 2018; Franceschi and Campisi, 2014; Furman et al., 2019). The persistence of inflammatogenic or metabolic stimuli may accelerate the generation and accumulation of SA lymphocyte subsets such as SA-T cells, Spt-GC B cells, and ABCs, which together may result in aggressive inflammatory tissue reactions such as TLTs and eventually organ dysfunction. The results of this study indicate the central role of the cognitive CD153/CD30 interaction in the development and activation of SA lymphocyte subsets, and Ab-mediated CD153 blockade may provide a promising means

Figure 5. Ab-mediated blockade of CD153 engagement suppresses the development of SA-T and GC B cells *in vivo*

(A and B) Characterization of 17D Ab. Binding of CD153-expressing 293FT cells to CD30-Ig (left) and cytolysis of CD153-expressing 3A9 T cell hybridoma (right) in the presence of indicated concentrations of control IgG, 17D, or RM153 (A). EC_{50} values for the CDC activity of 17D and RM153 were 5.7 and 0.04 μg/mL, respectively. Data (mean ± SD of triplicate samples) are representative of two independent experiments. Schematic representation of 17D epitope (B). TM domain, numbers; amino acid positions, arrows; putative CD30-binding residues shown by BLASTP at National Center for Biotechnology Information.

(C) Protocol of short-term Ab administration (upper left). B6 mice aged 9–10 weeks were administered R848 or saline three times a week for 1 month (n = 4 mice/group), followed by the injection of saline, control IgG, or 17D (n = 5 mice/group) for 1 week. Frequencies of SA-T cells and GC B cells (upper right; 1-month administration, lower left; 1-month + 1-week administration) as well as flow cytometry profiles and frequencies of Ki67+ cells in the indicated CD4+ T cell subpopulations (lower right; 1-month + 1-week administration) are shown.

(D) Effects of long-term administration of 17D. B6 mice aged 37–42 weeks were administered IgG or 17D three times a week for 1 month. Frequencies of indicated cell populations as well as OPN production by CD4+ T cells are shown (n = 5 mice/group).

(C and D) Data indicate the mean ± SEM. ns, not significant; *p < 0.05, **p < 0.01, ***p < 0.001, and ****p < 0.0001 by two-sided unpaired Student's t test (C and D), one-way ANOVA with Tukey's multiple comparison test, or Kruskal-Wallis test with Dunn's multiple comparison test (C). Please also see Figure S5.
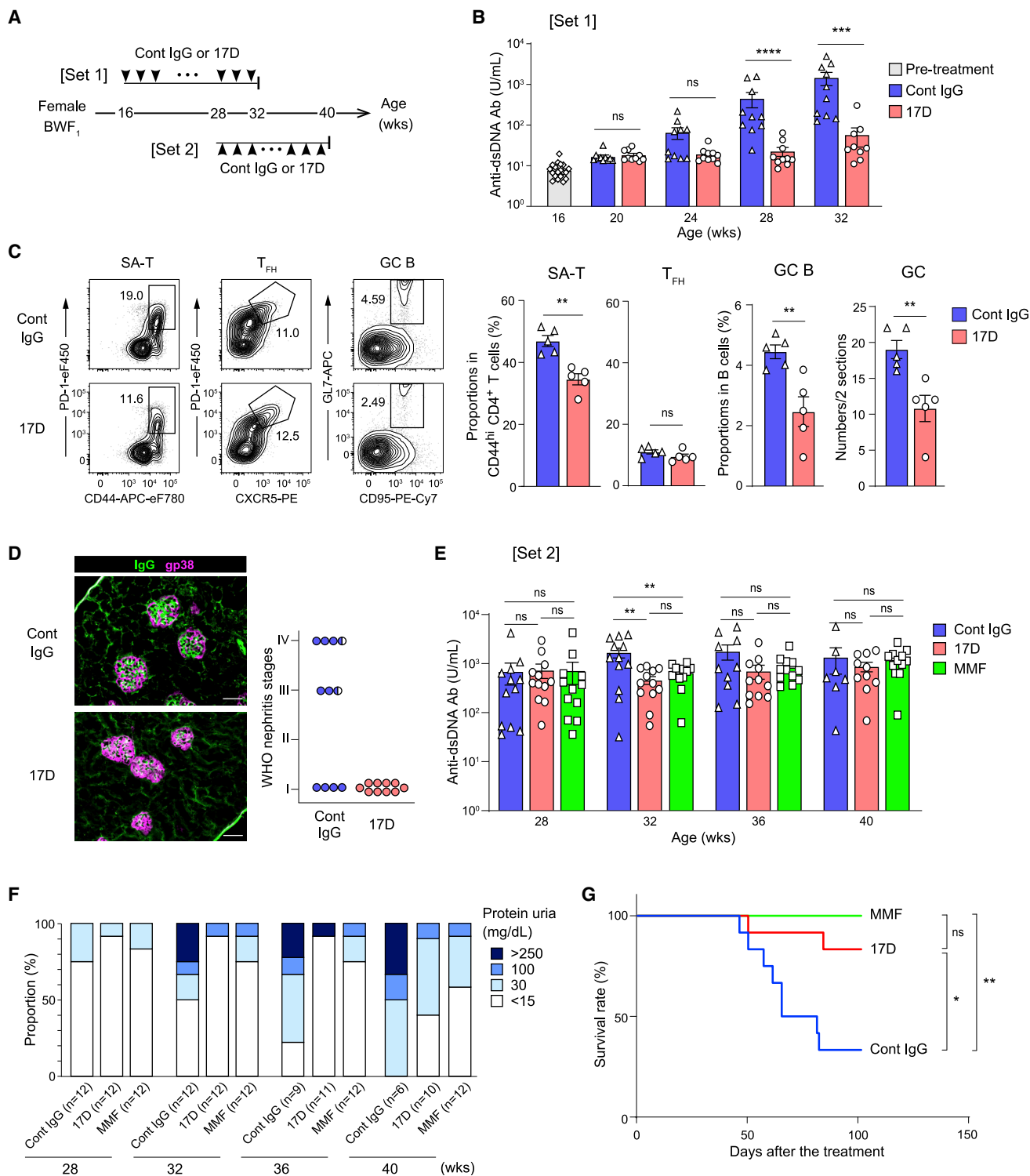
Figure 6. Amelioration of lupus development and progression with 17D administration in lupus-prone mice

(A) Protocols for Ab administration to female BWF₁ mice. Control mouse IgG or 17D were administered three times a week from the age of 16 to 34 weeks (Set 1: B–D) or from the age of 28 to 42 weeks (Set 2: E–G).

(B) Plasma concentrations of anti-dsDNA Abs (n = 10 mice/group).

(C) Flow cytometry profiles and frequencies of the indicated cell populations as well as the numbers of GCs in spleens (n = 5 mice/group).

(legend continued on next page)

of controlling various age-associated chronic inflammatory disorders and systemic autoimmunity in humans.

Limitations of the study

Our studies indicated intimate interaction between CD153^{+} SA-T cells and CD30^{+} B cells including Spt-GC B cells and ABCs for their reciprocal expansion. However, tissue localization of ABCs possibly with SA-T cells at some stages in their migration was not assessed because of the absence of the immunohistochemical staining to definitively distinguish ABCs. *In vitro* culture of ABCs in the presence of TLR7 agonists (Rubtsov et al., 2011) and CD153^{+} cells may help to assess the effect of CD30 signaling on this cell type as well. Although it may be advantageous to use primary CD153^{+} SA-T cells rather than cell lines to examine *in vivo* pathophysiology, the number of the primary cells available from the tissues is somehow limited. Thus, we used the cell lines in some biochemical assays such as co-immunoprecipitation. Considering the clinical application, it is intriguing that 17D Ab has little effect on the IgG Ab response against NP-OVA immunization in contrast to the prominent inhibitory effect on lupus pathogenesis, but further research is required to examine its potential effect on virus and mycobacterial infection.

STAR★METHODS

Detailed methods are provided in the online version of this paper and include the following:

AUTHOR CONTRIBUTIONS

Y.F. and M.H. designed and performed the experiments and wrote the manuscript. M.C. assisted with the experiments. K.S. participated in the experiments for assessing 17D Ab and lupus. M.M. performed confocal image analysis. Y.Y. provided both CD153- and CD30-knockout mice. H.Y. provided the RM153 antibody. D.K. provided the induced germinal center B cell culture system. N.M. supervised the overall studies and preparation of the manuscript.

REFERENCES

Adachi, K., and Davis, M.M. (2011). T-cell receptor ligation induces distinct signaling pathways in naive vs. antigen-experienced T cells. Proc. Natl. Acad. Sci. USA *108*, 1549–1554.

Alcover, A., Alarcón, B., and Di Bartolo, V. (2018). Cell biology of T cell receptor expression and regulation. Annu. Rev. Immunol. *36*, 103–125.

Babicki, S., Arndt, D., Marcu, A., Liang, Y., Grant, J.R., Maciejewski, A., and Wishart, D.S. (2016). Heatmapper: web-enabled heat mapping for all. Nucleic Acids Res. *44*, W147–W153.

Daniels, M.A., Teixeiro, E., Gill, J., Hausmann, B., Roubaty, D., Holmberg, K., Werlen, G., Holländer, G.A., Gascoigne, N.R.J., and Palmer, E. (2006). Thymic selection threshold defined by compartmentalization of Ras/MAPK signalling. Nature *444*, 724–729.

(D) Representative immunostaining of kidneys and staging of nephritis according to World Health Organization classification criteria (n = 10/group). IgG deposition (green), gp38 (magenta), glomerular epithelial marker. Scale bars, 50 μm; semi-filled circle, different classification in the two kidneys of single mouse.
(E) Plasma concentrations of anti-dsDNA Abs.
(F) Proportion of mice with indicated levels of proteinuria.
(G) Kaplan-Meier analyses of the survival.
(E–G) n = 12 mice/group at the initiation of experiments. MMF, mycophenolate mofetil.
(B, C, and E) Data indicate the mean ± SEM. ns, not significant; *p < 0.05, **p < 0.01, ***p < 0.001, and ****p < 0.0001 by two-sided Mann-Whitney U test (B), two-sided unpaired Student's t test (C), Kruskal-Wallis test, or one-way ANOVA with Tukey's multiple comparison test (E) and log-rank test with Bonferroni correction (F). Please also see Figure S6.

Domeier, P.P., Chodisetti, S.B., Soni, C., Schell, S.L., Elias, M.J., Wong, E.B., Cooper, T.K., Kitamura, D., and Rahman, Z.S.M. (2016). IFN-γ receptor and STAT1 signaling in B cells are central to spontaneous germinal center formation and autoimmunity. J. Exp. Med. 213, 715–732.

D'Oro, U., Munitic, I., Chacko, G., Karpova, T., McNally, J., and Ashwell, J.D. (2002). Regulation of constitutive TCR internalization by the zeta-chain. J. Immunol. 169, 6269–6278.

Elyahu, Y., Hekselman, I., Eizenberg-Magar, I., Berner, O., Strominger, I., Schiller, M., Mittal, K., Nemirovsky, A., Eremenko, E., Vital, A., et al. (2019). Aging promotes reorganization of the CD4 T cell landscape toward extreme regulatory and effector phenotypes. Sci. Adv. 5, eaaw8330.

Enyedy, E.J., Nambiar, M.P., Liossis, S.N., Dennis, G., Kammer, G.M., and Tsokos, G.C. (2001). Fc epsilon receptor type I gamma chain replaces the deficient T cell receptor zeta chain in T cells of patients with systemic lupus erythematosus. Arthritis Rheum. 44, 1114–1121.

Ferrucci, L., and Fabbri, E. (2018). Inflammageing: chronic inflammation in ageing, cardiovascular disease, and frailty. Nat. Rev. Cardiol. 15, 505–522.

Fillatreau, S., Manfroi, B., and Dörner, T. (2021). Toll-like receptor signalling in B cells during systemic lupus erythematosus. Nat. Rev. Rheumatol. 17, 98–108.

Franceschi, C., and Campisi, J. (2014). Chronic inflammation (inflammaging) and its potential contribution to age-associated diseases. J. Gerontol. A Biol. Sci. Med. Sci. 69 (Suppl 1), S4–S9.

Fukushima, Y., Minato, N., and Hattori, M. (2018). The impact of senescence-associated T cells on immunosenescence and age-related disorders. Inflamm. Regen. 38, 24.

Furman, D., Campisi, J., Verdin, E., Carrera-Bastos, P., Targ, S., Franceschi, C., Ferrucci, L., Gilroy, D.W., Fasano, A., Miller, G.W., et al. (2019). Chronic inflammation in the etiology of disease across the life span. Nat. Med. 25, 1822–1832.

Goronzy, J.J., and Weyand, C.M. (2019). Mechanisms underlying T cell ageing. Nat. Rev. Immunol. 19, 573–583.

Hamazaki, Y., Sekai, M., and Minato, N. (2016). Medullary thymic epithelial stem cells: role in thymic epithelial cell maintenance and thymic involution. Immunol. Rev. 271, 38–55.

Hao, Y., O'Neill, P., Naradikian, M.S., Scholz, J.L., and Cancro, M.P. (2011). A B-cell subset uniquely responsive to innate stimuli accumulates in aged mice. Blood 118, 1294–1304.

Hargreaves, P.G., and Al-Shamkhani, A. (2002). Soluble CD30 binds to CD153 with high affinity and blocks transmembrane signaling by CD30. Eur. J. Immunol. 32, 163–173.

Haswell, L.E., Glennie, M.J., and Al-Shamkhani, A. (2001). Analysis of the oligomeric requirement for signaling by CD40 using soluble multimeric forms of its ligand, CD154. Eur. J. Immunol. 31, 3094–3100.

Katsuyama, T., Tsokos, G.C., and Moulton, V.R. (2018). Aberrant T cell signaling and subsets in systemic lupus erythematosus. Front. Immunol. 9, 1088.

Li, G., Yu, M., Lee, W.W., Tsang, M., Krishnan, E., Weyand, C.M., and Goronzy, J.J. (2012). Decline in miR-181a expression with age impairs T cell receptor sensitivity by increasing DUSP6 activity. Nat. Med. 18, 1518–1524.

Liossis, S.N., Ding, X.Z., Dennis, G.J., and Tsokos, G.C. (1998). Altered pattern of TCR/CD3-mediated protein-tyrosyl phosphorylation in T cells from patients with systemic lupus erythematosus. Deficient expression of the T cell receptor zeta chain. J. Clin. Invest. 101, 1448–1457.

Liu, H., Rhodes, M., Wiest, D.L., and Vignali, D.A. (2000). On the dynamics of TCR:CD3 complex cell surface expression and downmodulation. Immunity 13, 665–675.

Minato, N., Hattori, M., and Hamazaki, Y. (2020). Physiology and pathology of T–cell aging. Int. Immunol. 32, 223–231.

Mittelbrunn, M., and Kroemer, G. (2021). Hallmarks of T cell aging. Nat. Immunol. 22, 687–698.

Nikolich-Žugich, J. (2014). Aging of the T cell compartment in mice and humans: from no naive expectations to foggy memories. J. Immunol. 193, 2622–2629.

Nojima, T., Haniuda, K., Moutai, T., Matsudaira, M., Mizokawa, S., Shiratori, I., Azuma, T., and Kitamura, D. (2011). In-vitro derived germinal centre B cells differentially generate memory B or plasma cells in vivo. Nat. Commun. 2, 465.

Ono, S., Ohno, H., and Saito, T. (1995). Rapid turnover of the CD3 zeta chain independent of the TCR-CD3 complex in normal T cells. Immunity 2, 639–644.

Palmer, S., Albergante, L., Blackburn, C.C., and Newman, T.J. (2018). Thymic involution and rising disease incidence with age. Proc. Natl. Acad. Sci. USA 115, 1883–1888.

Rubtsov, A.V., Rubtsova, K., Fischer, A., Meehan, R.T., Gillis, J.Z., Kappler, J.W., and Marrack, P. (2011). Toll-like receptor 7 (TLR7)-driven accumulation of a novel CD11c+ B-cell population is important for the development of autoimmunity. Blood 118, 1305–1315.

Rubtsov, A.V., Rubtsova, K., Kappler, J.W., Jacobelli, J., Friedman, R.S., and Marrack, P. (2015). CD11c-Expressing B cells are located at the T cell/B cell border in spleen and are potent APCs. J. Immunol. 195, 71–79.

Sakamoto, K., Fukushima, Y., Ito, K., Matsuda, M., Nagata, S., Minato, N., and Hattori, M. (2016). Osteopontin in spontaneous germinal centers inhibits apoptotic cell engulfment and promotes anti-nuclear antibody production in lupus-prone mice. J. Immunol. 197, 2177–2186.

Sato, K., Kato, A., Sekai, M., Hamazaki, Y., and Minato, N. (2017). Physiologic thymic involution underlies age-dependent accumulation of senescence-associated CD4(+) T cells. J. Immunol. 199, 138–148.

Sato, Y., Mii, A., Hamazaki, Y., Fujita, H., Nakata, H., Masuda, K., Nishiyama, S., Shibuya, S., Haga, H., Ogawa, O., et al. (2016). Heterogeneous fibroblasts underlie age-dependent tertiary lymphoid tissues in the kidney. JCI Insight 1, e87680.

Sato, Y., Oguchi, A., Fukushima, Y., Masuda, K., Toriu, N., Taniguchi, K., Yoshikawa, T., Cui, X., Kondo, M., Hosoi, T., et al. (2022). CD153-CD30 signaling promotes age-dependent tertiary lymphoid tissue expansion and kidney injury. J. Clin. Invest. 132, e146071.

Schindelin, J., Arganda-Carreras, I., Frise, E., Kaynig, V., Longair, M., Pietzsch, T., Preibisch, S., Rueden, C., Saalfeld, S., Schmid, B., et al. (2012). Fiji: an open-source platform for biological-image analysis. Nat. Methods 9, 676–682.

Sekai, M., Hamazaki, Y., and Minato, N. (2014). Medullary thymic epithelial stem cells maintain a functional thymus to ensure lifelong central T cell tolerance. Immunity 41, 753–761.

Shimatani, K., Nakashima, Y., Hattori, M., Hamazaki, Y., and Minato, N. (2009). PD-1+ memory phenotype CD4+ T cells expressing C/EBPalpha underlie T cell immunodepression in senescence and leukemia. Proc. Natl. Acad. Sci. USA 106, 15807–15812.

Shimozato, O., Takeda, K., Yagita, H., and Okumura, K. (1999). Expression of CD30 ligand (CD153) on murine activated T cells. Biochem. Biophys. Res. Commun. 256, 519–526.

Shinoda, K., Sun, X., Oyamada, A., Yamada, H., Kira, J.I., and Yoshikai, Y. (2016). Requirement of CD30 expression on CD4 T cells in the pathogenesis of experimental autoimmune encephalomyelitis. J. Neuroimmunol. 291, 39–45.

Shirakawa, K., Endo, J., Katsumata, Y., Yamamoto, T., Kataoka, M., Isobe, S., Yoshida, N., Fukuda, K., and Sano, M. (2017). Negative legacy of obesity. PLoS One 12, e0186303.

Shirakawa, K., Yan, X., Shinmura, K., Endo, J., Kataoka, M., Katsumata, Y., Yamamoto, T., Anzai, A., Isobe, S., Yoshida, N., et al. (2016). Obesity accelerates T cell senescence in murine visceral adipose tissue. J. Clin. Invest. 126, 4626–4639.

Song, W., Antao, O.Q., Condiff, E., Sanchez, G.M., Chernova, I., Zembrzuski, K., Steach, H., Rubtsova, K., Angeletti, D., Lemenze, A., et al. (2022). Development of Tbet- and CD11c-expressing B cells in a viral infection requires T follicular helper cells outside of germinal centers. Immunity 55, 290–307.e5.

Soni, C., Wong, E.B., Domeier, P.P., Khan, T.N., Satoh, T., Akira, S., and Rahman, Z.S.M. (2014). B cell-intrinsic TLR7 signaling is essential for the development of spontaneous germinal centers. J. Immunol. *193*, 4400–4414.

Stringer, C., Wang, T., Michaelos, M., and Pachitariu, M. (2021). Cellpose: a generalist algorithm for cellular segmentation. Nat. Methods *18*, 100–106.

Su, C.C., Chiu, H.H., Chang, C.C., Chen, J.C., and Hsu, S.M. (2004). CD30 is involved in inhibition of T-cell proliferation by Hodgkin's Reed-Sternberg cells. Cancer Res. *64*, 2148–2152.

Sun, X., Yamada, H., Shibata, K., Muta, H., Tani, K., Podack, E.R., and Yoshikai, Y. (2010). CD30 ligand/CD30 plays a critical role in Th17 differentiation in mice. J. Immunol. *185*, 2222–2230.

Tahir, S., Fukushima, Y., Sakamoto, K., Sato, K., Fujita, H., Inoue, J., Uede, T., Hamazaki, Y., Hattori, M., and Minato, N. (2015). A CD153+CD4+ T follicular cell population with cell-senescence features plays a crucial role in lupus pathogenesis via osteopontin production. J. Immunol. *194*, 5725–5735.

Tang, C., Yamada, H., Shibata, K., Muta, H., Wajjwalku, W., Podack, E.R., and Yoshikai, Y. (2008). A novel role of CD30L/CD30 signaling by T-T cell interaction in Th1 response against mycobacterial infection. J. Immunol. *181*, 6316–6327.

Valitutti, S., Müller, S., Cella, M., Padovan, E., and Lanzavecchia, A. (1995). Serial triggering of many T-cell receptors by a few peptide-MHC complexes. Nature *375*, 148–151.

Vinuesa, C.G., Linterman, M.A., Yu, D., and MacLennan, I.C.M. (2016). Follicular helper T cells. Annu. Rev. Immunol. *34*, 335–368.

Wiley, S.R., Goodwin, R.G., and Smith, C.A. (1996). Reverse signaling via CD30 ligand. J. Immunol. *157*, 3635–3639.

Xie, P. (2013). TRAF molecules in cell signaling and in human diseases. J. Mol. Signal. *8*, 7.

Yamaguchi, T., Morikawa, A., and Miyoshi, H. (2012). Comparison of gene-trapping efficiency between retroviral and lentiviral vectors in mouse embryonic stem cells. Biochem. Biophys. Res. Commun. *425*, 297–303.

Yanes, R.E., Gustafson, C.E., Weyand, C.M., and Goronzy, J.J. (2017). Lymphocyte generation and population homeostasis throughout life. Semin. Hematol. *54*, 33–38.

STAR★METHODS

KEY RESOURCES TABLE

REAGENT or RESOURCE	SOURCE	IDENTIFIER
Antibodies		
Anti-CD3 epsilon (145-2C11), FITC	BioLegend	Cat# 100306; RRID: AB_312671
Anti-CD3 epsilon (145-2C11), BV510	BioLegend	Cat# 100353; RRID: AB_2565879
Anti-CD3 epsilon (145-2C11), APC	BioLegend	Cat# 100312; RRID: AB_312677
Anti-CD3 epsilon (145-2C11), PE-Cy7	BioLegend	Cat# 100320; RRID: AB_312685
Anti-CD3 epsilon (145-2C11), PE	BioLegend	Cat# 100308; RRID: AB_312673
Anti-CD4 (GK1.5), Alexa Fluor 488	Invitrogen	Cat# 53-0041-82; RRID: AB_469893
Anti-CD4 (GK1.1), PE-Cy7	Invitrogen	Cat# 25-0041-82; RRID: AB_469576
Anti-CD4 (GK1.1), PerCP-Cy5.5	BioLegend	Cat# 100434; RRID: AB_893324
Anti-CD4 (GK1.1), vFluor 450	Tonbo Bioscience	Cat# 75-0041; RRID: AB_2621927
Anti-CD4 (GK1.5), APC-Cy7	BioLegend	Cat# 100414; RRID: AB_312699
Anti-CD4 (GK1.1), APC	BioLegend	Cat# 100412; RRID: AB_312697
Anti-CD8a (53-6.7), Pacific blue	BioLegend	Cat# 100725; RRID: AB_493425
Anti-CD11b (M1/70), FITC	BioLegend	Cat# 101206; RRID: AB_312789
Anti-CD11b (M1/70), vFluor 450	Tonbo Bioscience	Cat# 75-0112; RRID: AB_2621936
Anti-CD11b (M1/70), PerCP-Cy5.5	Invitrogen	Cat# 45-0112-82; RRID: AB_953558
Anti-CD11c (N418), PE-Cy7	BioLegend	Cat# 117317; RRID: AB_493569
Anti-CD25 (PC61.5), FITC	Tonbo Bioscience	Cat# 35-0251; RRID: AB_2621685
Anti-CD28 (37.51), PE	BioLegend	Cat# 102105; RRID: AB_312870
Anti-CD30 (mCD30.1), biotin	BioLegend	Cat# 102303; RRID: AB_2240925
Anti-CD30 (mCD30.1), APC	BioLegend	Cat# 102312; RRID: AB_2562412
Anti-CD44 (IM7), APC-eFluor 780	Invitrogen	Cat# 47-0441-82; RRID: AB_1272244
Anti-CD44 (IM7), BV510	BD Bioscience	Cat# 563114; RRID: AB_2738011
Anti-CD44 (IM7), PerCP-Cy5.5	BioLegend	Cat# 103032; RRID: AB_2076204
Anti-CD62L (MEL-14), FITC	Tonbo Biosciences	Cat# 35-0621; RRID: AB_2621697
Anti-CD62L (MEL-14), APC-Cy7	BioLegend	Cat# 104427; RRID: AB_830798
Anti-CD62L (MEL-14), PE-Cy7	eBioscience	Cat# 25-0621-82; RRID: AB_469633
Anti-CD95 (Jo2), PE-Cy7	BD Bioscience	Cat# 557653; RRID: AB_396768
Anti-CD121b (4E2), PE	BD Bioscience	Cat# 554450; RRID: AB_395399
Anti-CD138 (281-2), BV510	BioLegend	Cat# 142521; RRID: AB_2562727
Anti-CD153 (RM153), PE	Invitrogen	Cat# 12-1531-81; RRID: AB_465883
Anti-CD153 (RM153), biotin	eBioscience	Cat# 13-1531-81; RRID: AB_466622
Anti-B220 (RA3-6B2), APC-eFluor 780	eBioscience	Cat# 47-0452-82; RRID: AB_1518810
Anti-B220 (RA3-6B2), PerCP-Cy5.5	BioLegend	Cat# 103236; RRID: AB_893354
Anti-B220 (RA3-6B2), PE	eBioscience	Cat# 12-0452-83; RRID: AB_465672
Anti-B220 (RA3-6B2), APC	BioLegend	Cat# 103212; RRID: AB_312997
Anti-B220 (RA3-6B2), FITC	BD Bioscience	Cat# 553088; RRID: AB_394618
Anti-CXCR5 (2G8), biotin	BD Bioscience	Cat# 551960; RRID: AB_394301
Anti-GL7 (GL7), Alexa Fluor 647	eBioscience	Cat# 51-5902-80; RRID: AB_1311301
Anti-GL7 (GL7), FITC	BD Bioscience	Cat# 553666; RRID: AB_394981
Anti-Gr-1 (RB6-8C5), PE	eBioscience	Cat# 12-5931-81; RRID: AB_466044
Anti-Gr-1 (RB6-8C5), APC	BioLegend	Cat# 108411; RRID: AB_313376
Anti-Ki67 (16A8), PE	BioLegend	Cat# 652403; RRID: AB_2561524
Anti-Lag3 (C9B7W), PE-Cy7	BioLegend	Cat# 125226; RRID: AB_2715764
Anti-OPN, PE	R&D systems	Cat# IC808P; RRID: AB_10643832

(Continued on next page)

Continued

REAGENT or RESOURCE	SOURCE	IDENTIFIER
Anti-PD-1 (J43), eFluor 450	Invitrogen	Cat# 48-9985-82; RRID: AB_2574139
Anti-PD-1 (J43), PE-Cy7	Invitrogen	Cat# 25-9985-82; RRID: AB_10853805
Anti-Siglec-h (551), FITC	BioLegend	Cat# 129603; RRID: AB_1227760
Anti-TCR beta (H57-597), PE	BD Bioscience	Cat# 553172; RRID: AB_394684
Anti-TCR beta (H57-597)	Biolegend	Cat# 109254; RRID: AB_2813971
Anti-human IgG Fc (HP6017), PE	BioLegend	Cat# 409303; RRID: AB_10900424
Rat IgG2b isotype control (RKT4530), PE	BioLegend	Cat# 400607; RRID: AB_326551
Armenian hamster IgG isotype control (HTK888), PE	BioLegend	Cat# 400908; RRID: AB_326593
Armenian hamster IgG isotype control (HTK888), biotin	BioLegend	Cat# 400903
Syrian hamster IgG isotype control (SHG-1), PE	BioLegend	Cat# 402008
Anti-CD3 epsilon (CD3-12)	Cell Signaling Technology	Cat# 4443; RRID: AB_560945
Anti-CD3 delta	Proteintech	Cat# 16669-1-AP; RRID: AB_10598004
Anti-CD3 gamma (EPR4517)	abcam	Cat# ab134096
Anti-CD3 zeta (H146-968)	abcam	Cat# ab119827; RRID: AB_10902095
Anti-CD4	Proteintech	Cat# 11056-2-AP; RRID: AB_2073067
Anti-CD28 (D2Z4E)	Cell Signaling Technology	Cat# 38774; RRID: AB_2799141
Anti-CXCR4	Proteintech	Cat# 11073-2-AP; RRID: AB_2091813
Anti-GFP	Thermo Fisher Scientific	Cat# A11122; RRID: AB_221569
Anti-ERK1/2 (137F5)	Cell Signaling Technology	Cat# 4695; RRID: AB_390779
Anti-p-ERK1/2 (Tyr202/Tyr204) (D13.14.4E)	Cell Signaling Technology	Cat# 4370; RRID: AB_2315112
Anti-FcR gamma	Cell Signaling Technology	Cat# 20379
Anti-JNK	Cell Signaling Technology	Cat# 9252; RRID: AB_2250373
Anti-p-JNK (81E11)	Cell Signaling Technology	Cat# 4668; RRID: AB_823588
Anti-p38 (D13E1)	Cell Signaling Technology	Cat# 8690; RRID: AB_10999090
Anti-p-p38 (D3F9)	Cell Signaling Technology	Cat# 4511; RRID: AB_2139682
Anti-PD-1 (RMP1-14)	BioLegend,	Cat# 114101; RRID: AB_313572
Anti-PD-L2 (TY25)	BioLegend	Cat# 107208; RRID: AB_2162010
Anti-TCR alpha (H28-710)	Santa Cruz Biotechnology	Cat# sc-101410; RRID: AB_1130051
Anti-ZAP70 (D1C10E)	Cell Signaling Technology	Cat# 3165; RRID: AB_2218656
Anti-p-ZAP70 (Tyr319)/Syk (Tyr352) (65E4)	Cell Signaling Technology	Cat# 2717; RRID: AB_2218658
Anti-rabbit IgG (H+L), HRP	KPL	Cat# 074-1506; RRID: AB_2721169
Anti-rat IgG (H+L), HRP	KPL	Cat# 14-16-12
Anti-Armenian hamster IgG (H+L), HRP	Invitrogen	Cat# PA1-32045; RRID: AB_10985178
Anti-mouse IgG, HRP	Shibayagi	Cat# AKRDD-061
Anti-mouse IgG1, HRP	Southern biotech	Cat# 1070-05; RRID: AB_2650509
Anti-mouse IgG2b, HRP	Southern biotech	Cat# 1091-05; RRID: AB_2736842
Anti-mouse IgG3, HRP	Southern biotech	Cat# 1100-05; RRID: AB_2794573
Anti-TCR beta (H57-597), BV421	BioLegend	Cat# 109230; RRID: AB_2562562
Anti-CD3 epsilon (145-2C11)	BD Biosciences	Cat# 553058; RRID: AB_394591
Anti-B220 (RA3-6B2)	BioLegend	Cat# 103202; RRID: AB_312987
Anti-gp38 (eBio8.1.1)	eBioscience	Cat# 14-5381-82; RRID: AB_1210505
Anti-mouse IgG, Alexa Fluor 488	Invitrogen	Cat# A11029; RRID: AB_138404
Anti-rat IgG (H+L), Cy3	Jackson ImmunoResearch	Cat# 712-165-153; RRID: AB_2340667
Anti-Armenian hamster IgG (H+L), Alexa 647	Jackson ImmunoResearch	Cat# 127-605-160; RRID: AB_2339001
Anti-Syrian hamster IgG (H+L), DyLight 549	Jackson ImmunoResearch	Cat# 107-505-142; RRID: AB_2337475
Anti-CD28 (37.51)	Biolegend	Cat# 102116; RRID: AB_11147170

Continued

REAGENT or RESOURCE	SOURCE	IDENTIFIER
Anti-CD153 (RM153)	Dr. Hideo Yagita	N/A
Rat serum IgG control	Sigma-Aldrich	Cat# I4131; RRID: AB_1163627
Anti-CD153 (17D4-7)	This paper	N/A
mouse serum IgG control	Sigma-Aldrich	Cat# I5381; RRID: AB_1163670
Streptavidin, APC	BioLegend	Cat# 405207
Streptavidin, Alexa Fluor 488	Life Technologies	Cat# S32354; RRID: AB_2315383
Annexin V, APC	BD Biosciences	Cat# 550475; RRID: AB_2868885
Peanut agglutinin, biotin	Vector Laboratories	Cat# B-1075; RRID: AB_2313597
Biological samples		
SRBCs	Shimizu Laboratory Supplies	N/A
Chemicals, peptides, and recombinant proteins		
PMA	Sigma-Aldrich	Cat# P1585
Ionomycin	Sigma-Aldrich	Cat# I0634
Recombinant mouse IL-2	Tonbo Bioscience	Cat# 21-8021
Recombinant mouse IL-4	PeproTech	Cat# 214-14
Recombinant mouse IL-7	Tonbo Bioscience	Cat# 21-8071
Recombinant mouse IL-15	Tonbo Bioscience	Cat# 21-8153
Recombinant mouse IL-21	PeproTech	Cat# 210-21
NP-OVA	Biosearch Technologies	Cat# N-5051-10
NP30-BSA	Biosearch Technologies	Cat# N-5050H-10
NP4-BSA	Biosearch Technologies	Cat# N-5050L-10
Mitomycin C	Kyowa Hakko Kirin	N/A
R848	InvivoGen	Cat# tlrl-r848-5
PhosSTOP phosphatase inhibitor	Roche	Cat# 04906837001
Protease inhibitor cocktail	Nakalai	Cat# 25955-11
Low-Tox-M rabbit complement	Cedarlane	Cat# CL3051
Collagen type I, Rat Tail	Corning	Cat# 354236
Poly-L-lysine solution	Sigma-Aldrich	Cat# P48322
Critical commercial assays		
Amaxa SF Cell line 4D-Nucleofector X Kit	Lonza	Cat# V4XC-2024
PEI MAX, Transfection Grade	Polysciences	Cat# 24765-100
Lipofectamine 2000	Thermo Fisher	Cat# 11668027
BD Cytofix/Cytoperm Fixation/Permeabilization Solution Kit	BD Bioscience	Cat# 554714
Foxp3/Transcription Factor Staining Buffer Set	eBioscience	Cat# 00-5523-00
Trizol Reagent	Thermo FIsher	Cat# 15596018
SuperScript III Reverse Transcriptase	Invitrogen	Cat# 18080093
Transcriptor First Strand cDNA Synthesis Kit	Roche	Cat# 04897030001
DNase I, Amplification Grade	Thermo Fisher	Cat# 18068015
LightCycler 480 SYBR Green I Master	Roche	Cat# 04887352001
PowerUp SYBR Green Master Mix	Thermo Fisher	Cat# A25742
SMART-seq v4 Ultra Low Input RNA Kit	Takara Bio	Cat# 634888
Mouse Osteopontin DuoSet ELISA	R&D systems	Cat# DY441
Mouse IFN-gamma DuoSet ELISA	R&D systems	Cat# DY485
Mouse CCL3/MIP-1 alpha DuoSet ELISA	R&D systems	Cat# DY450
Mouse IL-4 DuoSet ELISA	R&D systems	Cat# DY404
ELISA MAX Deluxe SET Mouse TNF-alpha	Biolegend	Cat# 430904
ELISA assay for Mouse IL-2	MABTECH	Cat# 3441-1H-6

Continued

REAGENT or RESOURCE	SOURCE	IDENTIFIER
LBIS Mouse anti-ssDNA ELISA Kit	Shibayagi	Cat# AKRSD-051
LBIS Mouse anti-dsDNA ELISA Kit	Shibayagi	Cat# AKRDD-061
GFP-Trap Agarose Kit	ChromoTek	Cat# gtak-20
Protein G Sepharose 4 Fast Flow	GE Healthcare	Cat# 17-0618-02
SuperSignal West Pico or Femto PLUS maximum sensitivity chemiluminescent substrate	Thermo Fisher	Cat# 34577 or 34095
Mouse IgG ELISA Quantitation Set	Bethyl Laboratories	Cat# E90-131
Mouse IgG2c ELISA Quantitation Set	Bethyl Laboratories	Cat# E90-136
Deposited data		
Bulk RNA-seq data	This paper	GEO: GSE186221
Original code	This paper	Zenodo: https://doi.org/10.5281/zenodo.7017889
Experimental models: Cell lines		
EL4	Dr. Takashi Usui	N/A
3A9	Dr. Tatsuo Kinashi	RRID:CVCL_6239
40LB	Nojima et al. (2011)	RRID: CVCL_A6ZS
CD153/40LB	This paper	N/A
CD153Clov/EL4	This paper	N/A
CD153ΔCD/EL4	This paper	N/A
17D4-7	This paper	N/A
Experimental models: Organisms/strains		
Mouse: C57BL/6	Japan SLC	C57BL/6NCrSlc
Mouse: NZB x NZW F_1	Japan SLC	NZBWF1/Slc
Mouse: $CD153^{-/-}$	Tang et al. (2008)	N/A
Mouse: $CD30^{-/-}$	Shinoda et al. (2016)	N/A
Oligonucleotides		
qPCR primer sequences	This paper	See Method details
Recombinant DNA		
pcDNA3.1-CD153	This paper	N/A
pcDNA3.1-CD3γ	This paper	N/A
pcDNA3.1-CD3δ	This paper	N/A
pcDNA3.1-CD3ε	This paper	N/A
pcDNA3.1-CD3ζ	This paper	N/A
pcDNA3.1-FcRγ	This paper	N/A
pcDNA3.1-CD4	This paper	N/A
pcDNA3.1-PD-1	This paper	N/A
pcDNA3.1-PD-L2	This paper	N/A
pcDNA3.1-CXCR4	This paper	N/A
pcDNA3-Clover	Addgene	Cat# 40259; RRID: Addgene_40259
pCSIIpuro-Clover-CD153	This paper	N/A
pCSIIpuro-Clover-CD153ΔCD	This paper	N/A
Software and algorithms		
GraphPad Prism v9	GraphPad	https://www.graphpad.com/scientific-software/prism/
FlowJo	Treestar	https://www.flowjo.com/
ImageJ	NIH	https://imagej.nih.gov/ij/
Fiji	NIH	RRID: SCR_002285
Cellpose	GitHub	https://github.com/MouseLand/cellpose
MATLAB	Mathworks	RRID: SCR_001622

RESOURCE AVAILABILITY

Lead contact
Further information and requests for resources and reagents should be directed to and will be fulfilled by the lead contact, Yuji Fukushima (fukushima.yuji.4x@kyoto-u.ac.jp)

Materials availability
All unique/stable reagents generated in this study are available from the lead contact with a completed material transfer agreement.

Data and code availability
- Bulk RNA sequencing data have been deposited in the Gene Expression Omnibus database and are publicly available as of the data of publication. The accession number is listed in the key resources table.
- The original code has been deposited on Zenodo and are publicly available. DOI is listed in the key resources table.
- Any additional information required to reanalyze the data reported in this paper is available from the lead contact upon request.

EXPERIMENTAL MODEL AND SUBJECT DETAILS

Mice
WT B6 (female and male) and BWF$_1$ (female) mice were purchased from Japan SLC Inc. (Osaka, Japan). $CD153^{-/-}$ and $CD30^{-/-}$ B6 mice were as previously described (Shinoda et al., 2016; Tang et al., 2008). Female mice were used in animal experiments with the exception of Figure 1C (right; spleen cell count in male mice). The age of mice ranged from 8 to 78 weeks as indicated in the figures or figure legends. All mice were housed in specific pathogen-free conditions in the animal facility at Kyoto University (Kyoto, Japan). All animal experiments were performed strictly according to the institutional guidelines of Kyoto University Animal Ethics Committee.

Cell lines
Murine T-cell lymphoma EL4 cells and T-cell hybridoma 3A9 cells provided by T. Usui (Kyoto University) and T. Kinashi (Kansai Medical University, Osaka, Japan), respectively, were cultured in RPMI 1640 medium supplemented with 10% fetal calf serum (FCS), 50 μM β-mercaptoethanol, 100 U/mL penicillin, and 100 μg/mL streptomycin. 293T cells, 293FT cells (Thermo Fisher Scientific), and Balb/c 3T3 fibroblasts expressing both CD40L and BAFF (40LB cells) (Nojima et al., 2011) were maintained in Dulbecco's Modified Eagle Medium (DMEM) supplemented with 10% FCS, 100 U/mL penicillin, and 100 μg/mL streptomycin.

METHOD DETAILS

DNA constructs
pcDNA3.1-*CD153*, *CD3γ*, *CD3δ*, *CD3ε*, *CD3ζ*, *FcRγ*, *CD4*, *PD-1*, PD ligand 2 (*PD-L2*), and *CXCR4* were generated by cloning the relevant coding sequences, which were synthesized or PCR-amplified from the cDNA of mouse CD4$^+$ T cells into pcDNA3.1 (Thermo Fisher Scientific, Waltham, MA, USA). pcDNA3-Clover was purchased from Addgene (#40259; Watertown, MA, USA). pCSIIpuro-*Clover-CD153* was generated by insertion of a PCR-amplified DNA fragment encoding *Clover*, pentapeptide linker (GGSGG), and *CD153* from the N-terminus into pCSIIpuro (Yamaguchi et al., 2012). pCSIIpuro-*Clover-CD153ΔCD* was generated by deleting the cytoplasmic sequence of CD153 from pCSIIpuro-*Clover-CD153* by inverse PCR.

Transfection
Gene transfection was performed using the Amaxa SF Cell line 4D-Nucleofector X Kit and the 4D-Nucleofector System (Programs CM-120; EL4, CA-137; 3A9; Lonza, Rockville, MD, USA) for EL4 and 3A9 cells, and PEI MAX Transfection Reagent (Polysciences Inc., Warrington, PA, USA) or Lipofectamine 2000 (Thermo Fisher Scientific) for 293T, 293FT, and 40LB cells. Stable transfectants expressing CD153-Clover (CD153Clov), CD153ΔCD or CD153 proteins were obtained by incubation with puromycin (EL4; 2 μg/mL) for at least 2 weeks and subsequent FACS, or by magnetic cell separation (MACS system; Miltenyi Biotec, Gaithersburg, MD, USA) using PE-anti-CD153 Ab (RM153) and anti-PE Microbeads (Miltenyi). For the co-transfection assay, 293T cells were seeded at a density of 8 × 10^5 cells/well on collagen type I-coated 6-well plates (Corning Inc., Corning, NY, USA) the day before transfection. Cells were transfected with 2 μg pCSIIpuro-Clover-CD153 or pcDNA3-Clover in the additional presence of 2 μg pcDNA3.1-*CD3γ*, *CD3δ*, *CD3ε*, *CD3ζ*, *FcRγ*, *CD4*, *PD-1*, *PD-L2*, or *CXCR4*. After 2 days, the transiently transfected cells were prepared for immunoprecipitation as described below. All cell lines were maintained at 37°C in a humidified 5% CO$_2$ incubator.

Flow cytometry and cell sorting
Spleens were collected and mashed through a 70-mm cell strainer to yield a single-cell suspension. After the lysis of red blood cells in ACK lysing buffer, cells were treated with Fc blocking Ab (2.4G2) at 4°C for 15 min. The primary cells or cell lines shown above were stained at 4°C for 20 min, or in some cases for 40 min, with the following fluorophore-conjugated and biotinylated Abs: anti-CD3ε

(145-2C11), anti-CD153 (RM153), anti-PD-1 (J43), anti-CXCR5 (2G8), anti-CD62 (MEL-14), anti-CD4 (GK1.5), anti-CD44 (IM7), anti-CD25 (PC61.5), anti-CD121b (4E2), anti-lymphocyte activating 3 (Lag3) (C9B7W), anti-TCRβ (H57-597), anti-CD8a (53–6.7), anti-CD28 (37.51), anti-CD95 (Jo2), anti-GL7 (GL7), anti-B220 (RA3-6B2), anti-CD11b (M1/70), anti-CD11c (N418), anti-CD138 (281-2), anti-CD30 (mCD30.1), anti-Siglec-H (551), anti-Gr-1 (RB6-8C5), anti-human Ig (HP6017), Armenian hamster IgG isotype control (HKT888), Syrian hamster IgG isotype control (SHG-1), and rat IgG2b isotype control (RTK4530); all purchased from BioLegend (San Diego, CA, USA), BD Biosciences (Franklin Lakes, NJ, USA), eBioscience Inc. (San Diego, CA, USA), Invitrogen (Carlsbad, CA, USA), or Tonbo Biosciences (San Diego, CA, USA). After staining with biotinylated Abs, secondary staining with fluorophore-conjugated streptavidin (BioLegend) was performed at 4°C for 20 min. For intracellular staining with anti-OPN (polyclonal; R&D Systems, Minneapolis, MN, USA) and anti-Ki67 (16A8; BioLegend) Abs, the BD Cytofix/Cytoperm Fixation/Permeabilization Solution Kit (BD Biosciences) and Foxp3/Transcription Factor Staining Buffer Set (eBioscience Inc.) were used according to the manufacturers' instructions. Propidium iodide (PI) (Sigma-Aldrich, St. Louis, MO, USA) or Fixable Viability Dye eFluor 780 (Thermo Fisher Scientific) was used to exclude dead cells. These cells were analyzed and sorted using the FACSCanto II and FACS Aria II/III flow cytometers (BD Biosciences). Analyses of the flow cytometry data were performed using FlowJo software (TreeStar, Ashland, OR, USA).

CD4+ T-cell isolation and stimulation
CD4+ T cells were purified from splenic leukocytes by MACS using anti-CD4 (L3T4) microbeads (Miltenyi). For intracellular staining of OPN, the CD4+ T cells were incubated in RPMI 1640 medium containing 10% FCS, 50 μM β-mercaptoethanol, 100 U/mL penicillin, 100 μg/mL streptomycin, 20 ng/mL PMA, and 1 μg/mL ionomycin in the presence of brefeldin A for 7 h before the analyses. CD153+ SA-T (CD153+ PD-1+) and PD-1– CD25– cells in the CD44hi CD4+ B220– CD11b– gate were purified from the MACS-purified CD4+ T cell population using a FACS cell sorter. To enrich CD153+ SA-T cells without using anti-CD153 Ab, PD-1+ Lag3+ CD121b– CD25– cells were isolated with a FACS cell sorter. The isolated cells were incubated at a density of 5×10^4 cells/well in 96-well plates in the presence of varying combinations of plate-bound anti-CD3ε (1 μg/well), soluble anti-CD28 (2 μg/mL), plate-bound RM153 (2.5 μg/well), and plate-bound rat control IgG (2.5 μg/well) Abs for varying periods of time as indicated in the figures or figure legends. For the cell survival assay, the isolated CD153+ SA-T cells (4×10^5 cells/well) were incubated for 15 days in medium with or without 40 ng/mL IL-2 (Tonbo), 40 ng/mL IL-7 (Tonbo), 100 ng/mL IL-15 (Tonbo), 100 ng/mL IL-4 (PeproTech Inc., East Windsor, NJ, USA), or 100 ng/mL IL-21 (PeproTech). After staining with PI and APC-Annexin V (BD Biosciences), the frequency of viable cells were determined by FACS.

B-cell isolation and in vitro-iGB cell assay
The in vitro-iGB cell assay was performed as previously described with slight modification[4]. In brief, B cells were isolated from the splenic leukocytes of 8- to 9-week old B6 mice by MACS using FITC-anti-B220 Ab along with anti-FITC Microbeads (Miltenyi) and suspended in RPMI 1640 medium supplemented with 10% FCS, 50 μM β-mercaptoethanol, 10 mM HEPES, 1 mM sodium pyruvate, 100 U/mL penicillin, and 100 μg/mL streptomycin. The cells were seeded at a density of 3.3×10^5 cells/well in a 6-well plate in the presence of 1.0 ng/mL IL-4 and either 40LB or CD153/40LB cells (5×10^5 cells/well) that had been pretreated with 10 μg/mL mitomycin C for 2 h. The differentiating iGB cells were harvested to assess the expression of CD30 by FACS (daily until day 4), the viable cell number by cell counting (on day 3) and gene expression by qPCR (on day 3).

qPCR and bulk RNA sequencing analyses
RNA was extracted using TRIzol reagent (Thermo Fisher Scientific) and treated with DNase I (Themo Fisher Scientific), followed by purification by phenol/chloroform extraction and ethanol precipitation. For qPCR analyses, total RNA was reverse transcribed using SuperScript III (Invitrogen) or the Transcriptor First Strand cDNA Synthesis Kit (Roche). qPCR was performed with SYBR Green I Master mix (Roche, Basel, Switzerland) or PowerUp SYBR Green Master Mix (Applied Biosystems, Waltham, MA, USA). LightCycler 480 (Roche) and StepOne Plus Real-Time PCR System (Applied Biosystems) were used for data collection. The expression levels of each gene were normalized to that of *cyclophilin* (*Cyp*). The primer sequences were as follows: *Spp1* (forward: 5′-CCCGGTGAAAGT GACTGATT-3′, reverse: 5′-TTCTTCAGAGGACACAGCATTC-3′); *Sostdc1* (forward: 5′-AACAGCACCCTGAATCAAGC-3′, reverse: 5′-CAGCCCACTTGAACTCGAC-3′); *Tnfsf8* (forward: 5′-GAGGATCTCTTCTGTACCCTGAAA-3′, reverse: 5′-TTGGTATTGTTGA GATGCTTTGA-3′); *Irf4* (forward: 5′-AGCACCTTATGGCTCTCTGC-3′, reverse: 5′-TGACTGGTCAGGGGCATAAT-3′); *c-Myc* (forward: 5′-CGAAACTCTGGTGCATAAACTG-3′, reverse: 5′-GAACCGTTCTCCTTAGCTCTCA-3′); *Atf3* (forward: 5′-TGCCATCGGATG TCCTCT-3′, reverse: 5′-CGCCTCCTTTTCCTCTCAT-3′); *Tbx21* (forward: 5′-TCAACCAGCACCAGACAGAG-3′, reverse: 5′-AAA CATCCTGTAATGGCTTGTG-3′); *Cdkn2b* (forward: 5′-AATAACTTCCTACGCATTTTCTGC-3′, reverse: 5′-CCCTTGGCTTCAAGGTG AG-3′); *Cdkn1a* (forward: 5′-GGCCTCCCAGAGCATTCTA-3′, reverse: 5′-GTCCCCATCCCAGATAAGC-3′); *BclXL* (forward: 5′-AGG TATTGGTGAGTCGGATTGC-3′, reverse: 5′-TTGTTCCCGTAGAGATCCACAA-3′); *Bcl2a1a* (forward: 5′-TTTCCAGTTTTGTGGCA GAAT-3′, reverse: 5′-TCAAACTTCTTTATGAAGCCATCTT-3′); *Fcrg* (forward: 5′-ATCTCAGCCGTGATCTTGTTCT-3′, reverse: 5′-AC CATACAAAAACAGGACAGCAT-3′) and *Cyp* (forward: 5′-GACGAAGGTAGCCAGTCACAAG-3′, reverse: 5′-AATCAGGCCTGTG GAATGTGAG-3′). Bulk RNA sequencing was conducted by Macrogen Japan (Tokyo, Japan). RNA quality was assessed using the Agilent 2200 TapeStation (Agilent Technologies, Santa Clara, CA, USA). Libraries were generated using the SMART-seq v4 Ultra Low Input RNA Kit (Takara Bio USA, Inc., Mountain View, CA, USA) and then sequenced on the Illumina NovaSeq 6000 system. Differentially expressed genes were assessed using edgeR software. Heatmaps were drown using Heatmapper (Babicki et al., 2016).

Enzyme-linked immunosorbent assay

Cytokine and chemokine production in the cell culture supernatants were assessed with enzyme-linked immunosorbent assay (ELISA) kits (OPN, IFN-γ, Ccl3, IL-4 from R&D Systems; TNF-α from BioLegend; IL-2 from Mabtech, Mariemont, OH, USA). Plasma IgG titers were measured with ELISA kits (total IgG and IgG subclasses from Bethyl Laboratories, Montgomery, TX, USA; anti-single-stranded DNA Abs and anti-dsDNA Abs from Shibayagi, Gunma, Japan) or a standard method (anti-(4-hydroxy-3-nitrophenyl)acetyl 30 [NP30], anti-NP4, or anti-OVA Abs) as follows. Briefly, a 96-well Nunc Maxisorp plate (Thermo Fisher Scientific) was coated overnight with 10 μg/mL NP30-bovine serum albumin (BSA), NP4-BSA (Biosearch Technologies, Hoddesdon, UK), or OVA (Sigma-Aldrich) and then sequentially incubated with 1% BSA-phosphate-buffered saline (PBS) for 1 h, diluted serum samples for 1 h, and horseradish peroxidase (HRP)-anti-mouse IgG (Shibayagi) for 1 h. Plates were developed with TMB substrate (Life Technologies, Carlsbad, CA, USA) and read using the Sunrise Microplate Reader (Tecan, Mannerdorf, Switzerland) or a FlexStation 3 Microplate reader (Molecular Devices, San Jose, CA, USA).

Tissue immunostaining

Tissues were snap-frozen in optimum cutting temperature compound (Sakura Finetek, Torrance, CA, USA). Frozen sections with 6 μm thickness were fixed serially in 95% ethanol and 100% acetone. After blocking in 1% BSA-PBS, the sections were incubated with primary Abs and biotinylated peanut agglutinin (Vector Laboratories, Burlingame, CA, USA), followed by incubation with fluorophore-conjugated secondary Abs and streptavidin. Stained tissues were mounted with Mowiol 4–88 (Calbiochem, San Diego, CA, USA). The primary Abs used were: anti-B220 (RA3-6B2; BioLegend), anti-CD3ϵ (145-2C11; BD Biosciences), anti-gp38 (eBio8.1.1; eBioscience) and Alexa Fluor 488-anti-mouse IgG (polyclonal; Invitrogen). Images were acquired using the Zeiss Axiovert 200M microscope (Carl Zeiss, White Plains, NY, USA). Tile images of whole tissue sections were generated using the MosaiX tool of the Zeiss Axiovision software (Carl Zeiss).

Immunoprecipitation and immunoblotting

For the immunoprecipitation of Clover and CD153Clov proteins, EL4, CD153Clov/EL4 cells and co-transfected 293T cells were harvested, washed with PBS, and lysed in lysis buffer containing 1% CHAPS, 50 mM Tris-HCl (pH7.5), 150 mM NaCl, and protease inhibitor cocktail (Nacalai USA, Inc., Kyoto, Japan) for 30 min on ice. The cell lysates were IP'd using anti-green fluorescent protein (GFP) Nanobody-Coupled Beads (ChromoTek, Planegg, Germany) according to the manufacturer's instructions. For the immunoprecipitation of the TCR, CD153Clov/EL4 cells were added to multiple wells of round-bottom 96-well plates in the presence of plate-bound anti-CD3ϵ (1 μg/well), soluble anti-CD28 (2 μg/mL), plate-bound RM153, or plate-bound rat control IgG Abs (2.5 μg/well). After a brief spin, the cells were incubated for 5–90 min in a 37°C, 5% CO$_2$ incubator, immediately followed by lysis in buffer containing 1% Triton X-100, 50 mM Tris-HCl (pH 8.0), 150 mM NaCl, protease inhibitor cocktail, and PhosSTOP phosphatase inhibitor cocktail (Roche) for 30 min on ice. The cell lysates were pre-cleared with protein G beads (GE Healthcare, Chicago, IL, USA) and then IP'd with anti-TCRβ Ab (H57-597; BioLegend)-coupled beads. Proteins bound to the beads were eluted in sodium dodecyl sulfate sample buffer with heating. Co-IP'd proteins and/or aliquots of cell lysates were subjected to immunoblot analyses with the following primary Abs: anti-CD3γ (1:25,000, EPR4517) and CD3ζ (1:2,000, H146-968) were purchased from Abcam (Cambridge, MA, USA); anti-CD3ϵ (1:1,000, CD3-12), anti-FcRγ (polyclonal, 1:2,000), anti-CD28 (1:1,000, D2Z4E), anti-ZAP70 (1:4,000, D1C10E), anti-phosphorylated ZAP70 (anti-p-ZAP70) (Tyr319)/Syk (Tyr352) (1:2,000, 65E4), anti-ERK1/2 (1:2,000, 137F5), anti-p-ERK1/2 (Tyr202/Tyr204) (1:4,000, D13.14.4E), anti-p38 (1:2,000, D13E1), anti-p-p38 (1:2,000, D3F9), anti-JNK (polyclonal, 1:2,000), and anti-p-JNK (1:2,000, 81E11) were purchased from Cell Signaling Technology (Danvers, MA, USA); anti-TCRα (1:400, H28-710) was purchased from Santa Cruz Biotechnology (Dallas, TX, USA); anti-CD3δ (polyclonal, 1:1,000), anti-CD4 (polyclonal, 1:2,000), and anti-CXCR4 (polyclonal, 1:2,000) were purchased from Proteintech; anti-PD-1 (1:500, RMP1-14) and anti-PD-L2 (1:4,000, TY25) were purchased from BioLegend; anti-GFP (polyclonal, 1:2,000) was purchased from Thermo Fisher Scientific. Signals were developed with HRP-conjugated secondary Abs and the SuperSignal West Pico PLUS or Femto maximum sensitivity chemiluminescent substrate (Thermo Fisher Scientific). Images were captured using ImageQuant LAS500 (GE Healthcare). The intensity of the respective bands was analyzed using ImageJ software.

Microscopic observations of TCR and CD153Clov

CD153Clov/EL4 cells were stained with BV421-anti-TCRβ Ab on ice for 20 min, washed with 2% FCS-PBS, and suspended in phenol-red free RPMI 1640 medium containing 10% FCS, 50 μm β-mercaptoethanol, 100 U/mL penicillin, and 100 μg/mL streptomycin. The TCR-labeled cells were added at a density of 1 × 10^5 cells/well to a poly-L-lysine-coated glass-bottom 96-well plate in the presence or absence of plate-bound anti-CD3ϵ (1 μg/well), soluble anti-CD28 (2 μg/mL), plate-bound RM153 (2.5 μg/well), and rat control IgG (2.5 μg/well). After a brief spin, these cells were incubated for 30 min in a 37°C, 5% CO$_2$ incubator and then kept on ice until observation with the FV3000 confocal microscope (Olympus, Tokyo, Japan). Images of TCRβ and CD153Clov were analyzed by FIJI software (Schindelin et al., 2012). Briefly, after background subtraction, particles between 3 to 30 μm^2 were identified in TCRβ images to obtain the coordinates of the centroid. Cell boundaries determined with CD153Clov images using Cellpose (Stringer et al., 2021) were imported into FIJI and reduced by 1 pixel. By using the coordinates of the centroid and the cell boundary, the number of particles in each cell was counted by MATLAB (Mathworks Inc., Natick, MA).

Downregulation of cell surface TCR

Enriched CD153$^+$ SA-T cells were labeled with biotinylated anti-TCRβ Ab at 4°C for 20 min, washed with 2% FCS-PBS, and suspended in the culture medium. The TCR-labeled cells (5 × 10^4 cells/well) were stimulated on a 96-well plate in the presence of plate-bound anti-CD3ε (1 μg/well), soluble anti-CD28 (2 μg/mL), and either plate-bound RM153 (2.5 μg/well) or rat control IgG (2.5 μg/well) at 37°C for 1–3 h. These cells were harvested, washed, and stained with APC-streptavidin on ice for 20 min, followed by FACS analysis.

The monoclonal anti-CD153 Ab

Generation of anti-CD153 Abs and epitope mapping analyses were primarily performed by Kamakura Techno-Science Inc. (Kanagawa, Japan). In brief, a p3xFLAG-CMV-9 (Sigma-Aldrich)-based vector encoding the extracellular region of mouse CD153 (amino acid residues 68–239) with a neck region of SP-D (Haswell et al., 2001), 8×His- and 3× FLAG-tags was transfected in 293F cells using PEI MAX reagent. Soluble trimeric CD153 (sCD153) was purified from the culture supernatant using the TALON Metal Affinity Resin (Takara Bio), followed by size exclusion chromatography with Ultrogel AcA 34 Resin (Sigma-Aldrich). *CD153$^{-/-}$* mice were immunized subcutaneously with 100 μg of purified sCD153 emulsified with complete Freund's adjuvant (CFA). Splenocytes were fused with Sp2/0 myeloma cells in the presence of polyethylene glycol 1500 and cloned by limiting dilution, which yielded a hybridoma clone termed 17D4-7 (17D). Because 17D Ab recognizes mouse but not human CD153, the epitope was approximated and then narrowed down using mouse/human chimeric CD153 proteins (See Figure S5A). For approximation, vectors expressing seven types of chimeric proteins (soluble forms with a neck region of SP-D/Twin-strep-tag/8×His-tag) were transfected into 293F cells, and the produced proteins were purified from culture supernatants with TALON Resins. Streptavidin-treated 96-well plates (Thermo Fisher Scientific) were coated overnight with each purified protein (50 ng/well); and then sequentially incubated with diluted Blocking One (Nacalai) for 1–2 h, 17D Ab (5 ng/well) for 1 h, and HRP-anti-mouse IgG for 1 h. Plates were developed with TMB substrate and read on a plate reader to determine to which chimeric protein 17D can bind. For narrowing down, pcDNA3.1 vectors expressing two types of more segmentalized chimeric proteins (full-length forms) were transfected to 293T cells. The transiently transfected cells were harvested, stained with biotinylated 17D Ab along with PE-Streptavidin, followed by FACS analysis to determine which chimeric protein has the epitope.

Characterization of 17D Ab

To evaluate the blocking activity, CD153-expressing 293FT cells were incubated with serially diluted 17D, RM153, and mouse control IgG Abs (1–30 μg/mL) for 30 min on ice. After washing with 2% FCS-PBS, cells were reacted with recombinant CD30-Ig fusion protein (100 μg/sample) for 30 min and subsequently with PE-anti-human Ig Ab for 20 min on ice, followed by FACS analyses. To assess the CDC activities, CD153-expressing 3A9 cells (2 × 10^4 cells) were incubated in 1% FCS-RPMI 1640 containing either serially diluted 17D or RM153 Abs (17D, 0.1–30 μg/mL; RM153, 0.001–3 μg/mL) at 4°C for 1 h. After washing with 1% FCS-RPMI 1640, cells were incubated in medium supplemented with 10% Low-Tox-M rabbit complement (Cedarlane, Ontario, Canada) at 37°C for 30 min. Lysed cells were stained with PI and their frequency was determined by FACS.

In vivo administration of Abs

WT B6 and BWF$_1$ mice were intraperitoneally (*i.p.*) injected with anti-CD153 Abs (17D, RM153) and control serum IgG (mouse, rat; Sigma-Aldrich) at 500 μg per mouse three times per week for 1 week, 1 month, or several months as indicated in the figures or figure legends. In some cases, B6 mice were pre-treated with R848 (InvivoGen, San Diego, CA, USA) at 5 μg per mouse three times per week for 1 month. Spleens, plasma, or kidneys were collected from these mice for FACS, tissue immunostaining, ELISA, or staging of nephritis (Sapporo General Pathology Laboratory, Sapporo, Japan).

Immunization

WT and *CD153$^{-/-}$* mice were immunized *i.p.* with SRBCs (5 × 10^8 erythrocytes) or 100 μg of NP-OVA (Biosearch Technologies) emulsified in CFA. SRBC-immunized mice on day 7 after immunization were sacrificed for immunostaining of the spleens. Plasma was collected from NP-OVA-immunized mice to assess the titers of anti-NP30, anti-NP4 and anti-OVA Abs by ELISA.

QUANTIFICATION AND STATISTICAL ANALYSIS

Statistical analyses were performed using GraphPad Prism 9. Normality was assessed using the Shapiro–Wilk test. Two-sided, paired, and unpaired Student's t-test or nonparametric two-sided Mann–Whitney U test was used to compare two groups. One-way analysis of variance with Tukey's, Dunnett's, and Šidák's multiple comparison tests or the nonparametric Kruskal–Wallis test with Dunn's multiple comparison test was used to compare three or more groups. Log rank tests were performed to compare survival between mouse groups in Kaplan–Meier plots, with the individual p value multiplied by the number of comparisons (Bonferroni correction). The n represents number of mice used or biological replicates. $p < 0.05$ was considered statistically significant, unless stated otherwise. All experimental details can be found in the figure legends.